

The Parameterized Simulation of Electromagnetic Showers in Homogeneous and Sampling Calorimeters

G. Grindhammer¹ and S. Peters

Max-Planck-Institut für Physik
(Werner-Heisenberg-Institut)
Föhringer Ring 6
D-80805 München 40, Germany

Abstract: A general approach to a fast simulation of electromagnetic showers using parameterizations of the longitudinal and radial profiles in homogeneous and sampling calorimeters is described. The dependence of the shower development on the materials used and the sampling geometry is taken into account explicitly. Comparisons with detailed simulations of various calorimeters and with data from the liquid argon calorimeter of the H1 experiment are made.

1 Introduction

In calorimeter simulation different tasks can be distinguished: calorimeter studies, physics analysis, and feasibility studies. A detailed simulation, where all secondary particles are tracked individually down to some minimum energy and where the response is predicted from “first principles”, is required for accurate calorimeter studies. For physics analysis and feasibility studies large number of Monte Carlo events may have to be produced. Using individual particle tracking, the computing time needed for such kind of simulations increases approximately linear with the energy absorbed in the detector and can easily become prohibitive. Using parameterizations for electromagnetic (sub)showers can speed up the simulations considerably, without sacrificing precision. The high particle multiplicity in electromagnetic showers as well as their compactness and the good understanding of the underlying physics makes their parameterization advantageous.

Using an Ansatz by Longo and Sestili [1], a simple algorithm for the description of longitudinal shower profiles has been used successfully for the simulation of the UA1 calorimeter [2]. Later, this Ansatz has been extended to the simulation of individual

¹guenterg@desy.de

showers, taking their shower-to-shower fluctuation and correlations consistently into account [3, 4, 5]. For the parameterized simulation of radial energy profiles no conclusive procedure has been established until now.

In homogeneous media, a scaling of the longitudinal and radial profiles in radiation lengths and Molière radii respectively does not lead to a material independent description of electromagnetic shower development. In sampling calorimeters, the shower shapes depend in addition on the sampling structure. We have extended the above Ansatz for parameterized simulation of longitudinal profiles by taking the material and geometry dependence of the parameters into account and developed a new algorithm to simulate radial energy distributions [6]. Correlations between the longitudinal and radial shower development have been included.

2 Procedure

To arrive at a general description of electromagnetic shower development, we performed detailed Monte Carlo simulations, on a grid of $1.0 X_0$ in depth and 0.2 Molière radii laterally, for various homogeneous media and sampling calorimeters, using the GEANT package [7]. The materials used were Cu, Fe, W, Pb, U, and scintillator and liquid argon. In a first step only average shower profiles in homogeneous media were analyzed, from which scaling laws for the material and energy dependence of the parameters have been extracted. Starting from the relations which describe the average behavior of the parameterized quantities, we developed parameterizations for individual electromagnetic showers in homogeneous calorimeters, taking fluctuations and correlations into account.

The parameterizations in homogeneous media are a first approximation for electromagnetic shower development in sampling calorimeters, which are viewed as consisting of one single effective medium. The inhomogeneous material distribution in sampling calorimeters influences however the exact behavior of the shower shapes. This is explained mainly by the transition effect which depends on the shower depth [6, 8, 9]. These effects have been taken into account by adding geometry dependent terms to the parameterizations for homogeneous media, which can be easily calculated from the sampling geometry.

3 Parameterization Ansatz

The spatial energy distribution of electromagnetic showers is given by three probability density functions (pdf),

$$dE(\vec{r}) = E f(t)dt f(r)dr f(\phi)d\phi, \quad (1)$$

describing the longitudinal, radial, and azimuthal energy distributions. Here t denotes the longitudinal shower depth in units of radiation length, r measures the radial distance from the shower axis in Molière units, and ϕ is the azimuthal angle. The start of the shower is defined by the space point, where the first electron or positron bremsstrahlung

process occurs. A gamma distribution is used for the parameterization of the longitudinal shower profile, $f(t)$. The radial distribution, $f(r)$, is described by a two-component Ansatz. In ϕ , it is assumed that the energy is distributed uniformly: $f(\phi) = 1/2\pi$.

3.1 Longitudinal shower profiles – homogeneous media

It is well known that average longitudinal shower profiles can be described by a gamma distribution [1]:

$$\left\langle \frac{1}{E} \frac{dE(t)}{dt} \right\rangle = f(t) = \frac{(\beta t)^{\alpha-1} \beta \exp(-\beta t)}{\Gamma(\alpha)}. \quad (2)$$

The center of gravity, $\langle t \rangle$, and the depth of the maximum, T , can be calculated from the shape parameter α and the scaling parameter β according to

$$\langle t \rangle = \frac{\alpha}{\beta} \quad (3)$$

$$T = \frac{\alpha - 1}{\beta}. \quad (4)$$

Longitudinal electromagnetic shower development in homogeneous media had been studied analytically by Rossi [10]. An important result of the calculations using “Rossi Approximation B” is that longitudinal shower moments are equal in different materials, provided one measures all lengths in units of radiation length (X_0) and energies in units of the critical energy (E_c). Numerically, E_c can be calculated according to [11]

$$E_c = 2.66 \left(X_0 \frac{Z}{A} \right)^{1.1}. \quad (5)$$

For the depth of the shower maximum

$$T \propto \ln y = \ln \frac{E}{E_c} \quad (6)$$

is predicted [10].

It is therefore desirable to use T in the parameterization. This is demonstrated in Fig.1, where the average depth of the shower maximum for various homogeneous media², T_{hom} , is plotted versus y , in the energy range from 1 to 100 GeV. As a second variable α is used. In this case the parameterization depends on the charge number Z of the medium, as can be seen in Fig.2. The lines in both figures correspond to fits to GEANT simulations according to

$$T_{hom} = \ln y + t_1 \quad (7)$$

$$\alpha_{hom} = a_1 + (a_2 + a_3/Z) \ln y. \quad (8)$$

² The index “hom” in the following formulae indicates the validity for homogeneous media. For sampling calorimeters the index “sam” will be used.

The values of the coefficients are given in Appendix, where all formulae and numbers, which will be given in the following, are summarized.

Assuming that also individual profiles can be approximated by a gamma distribution, the fluctuations and correlations can be taken into account consistently (for details refer to [5]). For each single GEANT-simulated shower, T and α are determined by fitting a gamma distribution. The logarithms of T and α are used for the parameterization since they are found to be approximately normal distributed. For the parameterization of $\langle \ln T_{hom} \rangle$ and $\langle \ln \alpha_{hom} \rangle$ the logarithms of equations 7 and 8 are used. The y -dependence of the fluctuations can be described by

$$\sigma = (s_1 + s_2 \ln y)^{-1}. \quad (9)$$

The correlation between $\ln T_{hom}$ and $\ln \alpha_{hom}$ is given by

$$\rho(\ln T_{hom}, \ln \alpha_{hom}) \equiv \rho = r_1 + r_2 \ln y. \quad (10)$$

The dependence of these quantities on y is shown in Fig.3 for various materials together with the parameterizations (see Appendix A.1.2).

From these formulae, correlated and varying parameters α_i and β_i are generated according to

$$\begin{pmatrix} \ln T_i \\ \ln \alpha_i \end{pmatrix} = \begin{pmatrix} \langle \ln T \rangle \\ \langle \ln \alpha \rangle \end{pmatrix} + C \begin{pmatrix} z_1 \\ z_2 \end{pmatrix} \quad (11)$$

with

$$C = \begin{pmatrix} \sigma(\ln T) & 0 \\ 0 & \sigma(\ln \alpha) \end{pmatrix} \begin{pmatrix} \sqrt{\frac{1+\rho}{2}} & \sqrt{\frac{1-\rho}{2}} \\ \sqrt{\frac{1+\rho}{2}} & -\sqrt{\frac{1-\rho}{2}} \end{pmatrix}$$

and $\beta_i = (\alpha_i - 1)/T_i$ and z_1 and z_2 are standard normal distributed random numbers. The longitudinal energy distribution is evaluated³ by integration in steps of $\Delta t = t_j - t_{j-1} = 1X_0$,

$$dE(t) = E \int_{t_{j-1}}^{t_j} \frac{(\beta_i t)^{\alpha_i - 1} \beta_i \exp(-\beta_i t)}{\Gamma(\alpha_i)} dt.$$

It is worthwhile to mention that only one of the five quantities needed, $\langle \ln \alpha_{hom} \rangle$, depends explicitly on the material, while for the other four this dependence is absorbed by using y instead of E .

In Fig.4 longitudinal profiles of GEANT and parameterized simulations for a lead glass calorimeter (SF5) are compared. Shown are the mean profiles and the mean + 1 RMS in each X_0 interval. While the means are in perfect agreement, the fluctuations are underestimated by the parameterized simulations at low energies, indicating that the description of individual profiles by gamma distributions becomes a worse approximation with decreasing shower energy. Comparisons for other materials (Fe, Cu, W, Pb, U) are of comparable quality as those in Fig.4 [6]. In the next sections we will show, how the sampling fluctuations in sampling calorimeters can be used to improve the shape fluctuations at low energies.

³ The GAMDIS function of the CERN computer library is used.

3.2 Sampling fluctuations

In fast simulations, sampling calorimeters consisting of a complicated but repetitive sampling structure are usually described by one single effective medium (the formulae to compute effective material parameters are summarized in Appendix A.2.1). The sampling fluctuations, the scaling of the deposited energy to the visible energy using an appropriate sampling fraction, and the effects of the sampling structure have to be considered in parameterized simulations explicitly.

The simulation of sampling fluctuations are done conveniently with a gamma distribution:

$$G(a, b) = \frac{x^{a-1} b e^{-bx}}{\Gamma(a)} \quad (12)$$

with

$$\langle x \rangle = \frac{a}{b}, \quad \sigma^2(x) = \frac{a}{b^2}. \quad (13)$$

The energy in each longitudinal integration step, $dE(t)$, is fluctuated⁴ according to equation 12 choosing

$$a = \frac{dE(t)}{c^2} \text{ and } b = \frac{1}{c^2}. \quad (14)$$

It is then easy to show that the central limit theorem will ensure the total energy to be normal distributed obeying the usual formula for the sampling fluctuations:

$$\frac{\sigma}{E} = \frac{c}{\sqrt{E}}. \quad (15)$$

Using this procedure the occurrence of negative energies is automatically avoided. Additional fluctuations of the longitudinal shape are introduced, leading to a better agreement in the shape fluctuations. This method is also used to fluctuate energy depositions of real particles (electrons, hadrons), when they are tracked individually through an effective homogeneous volume.

3.3 Longitudinal shower profiles – sampling calorimeters

The inhomogeneous material distribution in sampling calorimeters influences the exact behavior of the shower shapes. In the first stages of electromagnetic shower development the signal is dominated by electrons and positrons. Behind the shower maximum low energetic photons become more and more important. The transition effect, being explained mainly by the absorption properties of low energetic photons, must in turn depend on the shower depth. Consequently, the signal ratio of electrons to minimum ionizing particles, e/mip , decreases continuously as the shower propagates longitudinally. Thus the signal maximum in a sampling calorimeter occurs at an earlier depth than expected for a homogeneous calorimeter with the same effective material properties. This can be seen from Fig.5 (left upper corner), where $\langle \ln T \rangle$ for homogeneous media is compared to the

⁴ The RANGAM function of the CERN computer library is used.

values in five different sampling calorimeters. In addition, the amount of the shift of $\langle \ln T \rangle$ depends on the exact geometrical arrangement.

The parameterization of the longitudinal shape as given in section 3.1 for homogeneous media can therefore not be used for sampling calorimeters directly. Instead it may be understood as a first approximation to which geometry dependent corrections have to be added. We use the sampling frequency

$$F_S = \frac{X_{0,eff}}{d_a + d_p} \quad (16)$$

and the value of e/mip (averaged over the shower depth) to account for the shower depth dependence of the transition effect. d_a and d_p denote the thickness of the active and passive layers, respectively. If e/mip is not known, a sufficiently good approximation for many calorimeters [12] with charge numbers Z_p and Z_a is given by

$$\hat{e} = \frac{1}{1 + 0.007(Z_p - Z_a)} \approx \frac{e}{mip}. \quad (17)$$

Averaged over the whole shower, e/mip remains energy independent for $E \gtrsim 1$ GeV.

The average longitudinal profiles can now be parameterized according to

$$T_{sam} = T_{hom} + t_1 F_S^{-1} + t_2 (1 - \hat{e}) \quad (18)$$

$$\alpha_{sam} = \alpha_{hom} + a_1 F_S^{-1}, \quad (19)$$

and the quantities used for the simulation of individual showers are given by

$$\langle \ln T_{sam} \rangle = \ln \left(\exp(\langle \ln T_{hom} \rangle) + t_1 F_S^{-1} + t_2 (1 - \hat{e}) \right) \quad (20)$$

$$\langle \ln \alpha_{sam} \rangle = \ln \left(\exp(\langle \ln \alpha_{hom} \rangle) + a_1 F_S^{-1} \right). \quad (21)$$

The fluctuations, $\sigma(\ln T_{sam})$, $\sigma(\ln \alpha_{sam})$ and the correlation, $\rho(\ln T_{sam}, \ln \alpha_{sam})$, are described with the help of the same formulae as in the case of homogeneous media (see Appendix A.2.2 and A.2.3).

Fig.5 summarizes the parameterization for sampling calorimeters. The expectation value of $\ln T$ no longer scales with y . The expectation value of $\ln \alpha$ depends on the material and the sampling geometry. The fluctuations and correlations of the parameters can still be approximated without any explicit material or geometry dependence.

In Figs.6 to 8 GEANT and parameterized simulations of the lead liquid argon calorimeter (IFE) of the H1 experiment [13, 6] are compared. The GEANT simulations were performed with low energy cuts (e -cut= 200 keV, γ -cut= 10 keV) and a detailed geometry description, including for example copper pads and G10 layers. These simulations were *not* used to tune the parameterizations. Both, average longitudinal profiles and their fluctuations (including sampling fluctuations) are in very good agreement (see Fig.6). The energy containment (see Fig.7) and the energy resolution (see Fig.8) as a function of the longitudinal calorimeter length are also well predicted. Comparisons with detailed simulations of other calorimeters (Fe-LAr, Cu-Sc, W-LAr, Pb-LAr, U-Sc) show a comparably good performance [6].

3.4 Radial shower profiles – homogeneous media

Average radial energy profiles,

$$f(r) = \frac{1}{dE(t)} \frac{dE(t, r)}{dr}, \quad (22)$$

at different shower depths in pure uranium are presented in Fig.9. These profiles show a distinct maximum in the core of the shower which vanishes with increasing shower depth. In the tail ($r \gtrsim 1R_M$) the distribution looks nearly flat at the beginning ($1 - 2X_0$), becomes steeper at moderate depths ($5 - 6X_0$, $13 - 14X_0$), and becomes flat again ($22 - 23X_0$). A variety of different functions can be found in the literature to describe radial profiles [14, 15, 16, 17, 18, 5]. We use the following two component Ansatz, an extension of [5]:

$$\begin{aligned} f(r) &= pf_C(r) + (1 - p)f_T(r) \\ &= p \frac{2rR_C^2}{(r^2 + R_C^2)^2} + (1 - p) \frac{2rR_T^2}{(r^2 + R_T^2)^2} \end{aligned} \quad (23)$$

with

$$0 \leq p \leq 1.$$

Here R_C (R_T) is the median of the core (tail) component and p is a probability giving the relative weight of the core component. For the shower depth $1 - 2X_0$ the distributions $f(r)$, $pf_C(r)$, and $(1 - p)f_T(r)$ are also indicated in Fig.9.

The evolution of R_C , R_T , and p with increasing shower depth is shown in Fig.10 for 100 GeV showers in iron and uranium. We use the variable $\tau = t/T$, which measures the shower depth in units of the depth of the shower maximum, to generalize the radial profiles. This makes the parameterization more convenient and separates the energy and material dependence of various parameters. The median of the core distribution, R_C , increases linearly with τ . The weight of the core, p , is maximal around the shower maximum, and the width of the tail, R_T , is minimal at $\tau \approx 1$. This behavior can be traced back to the radial profiles shown in Fig.9.

The following formulae are used to parameterize the radial energy density distribution for a given energy and material:

$$R_{C,hom}(\tau) = z_1 + z_2\tau \quad (24)$$

$$R_{T,hom}(\tau) = k_1 \{ \exp(k_3(\tau - k_2)) + \exp(k_4(\tau - k_2)) \} \quad (25)$$

$$p_{hom}(\tau) = p_1 \exp \left\{ \frac{p_2 - \tau}{p_3} - \exp \left(\frac{p_2 - \tau}{p_3} \right) \right\} \quad (26)$$

The parameters $z_1 \cdots p_3$ are either constant or simple functions of $\ln E$ or Z (see Appendix A.1.3 for details). The complicated evolution of R_T and p with the shower depth and the dependence on the material can be explained mainly with the propagation of low energetic photons [6]. The offset in R_T between iron and uranium (Fig.10) for example, indicating a wider distribution in iron, reflects the difference in the mean free path, which for 1 MeV

photons is approximately twice as long in iron as in uranium, if lengths are measured in Molière units.

We found a good agreement of mean radial profiles between parameterized and detailed simulations in Fe, Cu, W, Pb, and U absorbers for energies between 0.4 and 400 GeV. This is demonstrated in Fig.12, where radial profiles in various shower depths are compared for 40 GeV showers in lead and 100 GeV showers in uranium.

The introduction of radial shape fluctuations has to be considered with some care. Even if no fluctuations of $f(r)$ are simulated explicitly, the radial energy profile at a given shower depth will fluctuate, because the shower maximum T and thus τ varies from shower to shower. Another source of radial fluctuations arises from the method, which we have adopted for the simulation of radial distributions. The energy content of a longitudinal interval of length 1 X_0 , $dE(t)$, is calculated from the actual longitudinal energy density distribution as described in section 3.1. This energy is divided into $N_S(t)$ discrete spots of energy $E_S = dE(t)/N_S(t)$, which are distributed radially according to $f(r)$ using a Monte Carlo method. This can be done easily since the pdfs, $f_C(r)$ and $f_T(r)$, can be integrated and inverted:

$$F(r) = \int_0^r \frac{2r'R^2}{(r'^2 + R^2)^2} dr' = \frac{r^2}{r^2 + R^2} \quad (27)$$

$$F^{-1}(u) = R\sqrt{\frac{u}{1-u}}. \quad (28)$$

Random radii are generated according to $f(r)$ in the following way, using two normal distributed random numbers v_i and w_i :

$$r_i = \begin{cases} R_C \sqrt{\frac{v_i}{1-v_i}}, & \text{if } p < w_i \\ R_T \sqrt{\frac{v_i}{1-v_i}}, & \text{else.} \end{cases}$$

This method leads to additional fluctuations in the energy content of every radial interval which follow a binomial distribution. Thus, the relation

$$\frac{\sigma^2(\epsilon)}{\langle \epsilon \rangle (1 - \langle \epsilon \rangle)} = \text{const} = N_S^{-1} \quad (29)$$

describes the contribution to radial shape fluctuations produced by the Monte Carlo method in each longitudinal integration interval. Here ϵ denotes the energy in a given radial interval at a given shower depth:

$$\langle \epsilon \rangle \equiv \int_{r_1}^{r_2} f(r) dr = \frac{dE(t, r)}{dE(t)}. \quad (30)$$

We investigated the possibility to tune $N_S(t)$ in each longitudinal interval to match the radial shape fluctuations observed in detailed GEANT simulations⁵. As an example, the

⁵De Angelis et al. have used a similar method to reproduce shape fluctuations [19].

quantity $\sigma^2(\epsilon)/(\langle\epsilon\rangle(1-\langle\epsilon\rangle))$ at $t = 5 - 6X_0$ is displayed in Fig.11 for detailed simulations and parameterized ones without any radial shape fluctuations. The difference of these curves, which is also shown in Fig.11, is approximately constant and determines N_S^{-1} in equation 29 (note that the variance is additive). We found that a constant contribution to $\sigma^2(\epsilon)/(\langle\epsilon\rangle(1-\langle\epsilon\rangle))$ can be used to match the total radial shape fluctuations to a good approximation at all shower depths.

Summing $N_S(t)$ over all shower depth, the total number of spots, N_{Spot} , needed for one shower can be obtained and parameterized according to

$$N_{Spot} = 93 \ln(Z) E^{0.876}. \quad (31)$$

To find the number of spots for each longitudinal integration interval, the density distribution $1/N_{Spot} dN_S(t)/dt$ in Fig.11 is parameterized. It is described by a gamma distribution with parameters, which are given by the corresponding longitudinal energy profile:

$$T_{Spot} = T_{hom}(0.698 + 0.00212Z) \quad \text{and} \quad (32)$$

$$\alpha_{Spot} = \alpha_{hom}(0.639 + 0.00334Z). \quad (33)$$

The total fluctuations obtained with this method are compared in Fig.12 by adding 1 RMS to the mean profiles.

Additional correlations between longitudinal and radial shower development are taken into account by introducing a correlation between the radial pdfs and the actual center of gravity,

$$\langle t \rangle_i = \frac{\alpha_i}{\beta_i} = T_i \frac{\alpha_i}{\alpha_i - 1},$$

of an individual shower. This is done by replacing τ in equations 24, 25, and 26 by τ_i :

$$\tau = \frac{t}{T} \longrightarrow \tau_i = \frac{t}{\langle t \rangle_i} \frac{\exp(\langle \ln \alpha \rangle)}{\exp(\langle \ln \alpha \rangle) - 1}. \quad (34)$$

The need to introduce these correlations is demonstrated in Fig.13, where integrated radial profiles are shown, which were calculated by summing over all longitudinal layers. Note that the mean integrated profiles,

$$\left\langle \frac{1}{E} \frac{dE(r)}{dr} \right\rangle,$$

are independent of energy, which is well reproduced by the parameterized simulation. The relative fluctuations of these distributions,

$$\hat{\sigma}(r) \equiv \frac{\sigma_{RMS}}{\left\langle \frac{1}{E} \frac{dE(r)}{dr} \right\rangle},$$

are shown using both, τ and τ_i , in calculating the radial profiles. Only the simulations using τ_i are able to predict the fluctuations observed with GEANT correctly.

For clarity, we summarize the steps of our algorithm as follows: Determine the energy $dE(t)$ within one longitudinal integration interval as described in section 3.1. In case of sampling calorimeters apply sampling fluctuations on $dE(t)$. Evaluate the number of spots needed to reproduce radial shape fluctuations in this interval according to

$$N_S(t) = N_{Spot} \int_{t_{j-1}}^{t_j} \frac{(\beta_{Spot} t)^{\alpha_{Spot}-1} \beta_{Spot} \exp(-\beta_{Spot} t)}{\Gamma(\alpha_{Spot})} dt.$$

Distribute the spots with energy $E_S = dE(t)/N_S(t)$ radially according to $f(r)$ as described above and uniformly in ϕ and in the longitudinal interval Δt . Finally transform the spot coordinates $(E_S, t[X_0], r[R_M], \phi)$ into the detector reference system (E_S, x, y, z) .

3.5 Radial shower profiles – sampling calorimeters

The influence of the exact geometry on radial energy profiles is rather small. At the start of the shower the profiles look a bit smoother than in homogeneous media. With increasing shower depth they approach the shapes that are expected for homogeneous media with the appropriate effective material. These small deviations have been taken into account by the following corrections to the mean profiles:

$$R_{C,sam} = R_{C,hom} + z_1(1 - \hat{e}) + z_2 F_S^{-1} \exp(-\tau_i) \quad (35)$$

$$R_{T,sam} = R_{T,hom} + k_1(1 - \hat{e}) + k_2 F_S^{-1} \exp(-\tau_i) \quad (36)$$

$$p_{sam} = p_{hom} + (1 - \hat{e})(p_1 + p_2 F_S^{-1} \exp(-(\tau_i - 1)^2)) \quad (37)$$

using again the sampling frequency F_S and e/mip (see Appendix A.2.4).

The total number of spots needed to simulate the radial shape fluctuations is much smaller than in the case of homogeneous media and no longer depends sensitively on the materials used. Instead, the spot number can be parameterized by

$$N_{Spot} = \frac{10.3}{c} E^{0.959}, \quad (38)$$

where c measures the sampling fluctuations according to

$$\frac{\sigma}{E} = \frac{c}{\sqrt{E}}$$

(see Fig.14). The density distribution of the spot numbers is given in analogy to the homogeneous media by:

$$T_{Spot} = T_{sam}(0.831 + 0.0019Z) \quad \text{and} \quad (39)$$

$$\alpha_{Spot} = \alpha_{sam}(0.844 + 0.0026Z) \quad (40)$$

GEANT and parameterized simulations of mean radial profiles and their relative fluctuations,

$$\hat{\sigma}(t, r) = \frac{\sigma_{RMS}}{\left\langle \frac{1}{dE(t)} \frac{dE(t, r)}{dr} \right\rangle}, \quad (41)$$

are compared in Fig.15 and Fig.16 for the H1 liquid argon calorimeter (IFE) for various energies. The influence of radial leakage on containment and energy resolution is demonstrated in Fig.17 and Fig.18. The energy independence of the energy contained in a cylinder of radius r is well reproduced by the parameterized simulations. The energy resolution as defined in Fig.18 does not depend on radial leakage. As can be seen, this is correctly predicted by the parameterized simulation, when the correlation between the longitudinal and radial shower development is taken into account (by using τ_i).

4 Comparison with data

We have compared parameterized simulations with test beam data from the H1 calorimeter, which is made of lead and liquid argon in the electromagnetic sections [13, 6]. Modules of the inner forward (IFE), the forward barrel (FB1), and the central barrel (CB2/CB3) calorimeters have been studied. Electron beams in the energy range between 5 and 80 GeV entered the stacks under angles of 11° in the IFE and CB3, and under 35° in the FB1 calorimeter in a test set-up at CERN.

The energy resolution of the data can be described by

$$\frac{\sigma(E)}{\langle E \rangle} = \sqrt{\frac{c^2}{\langle E \rangle} + \frac{b^2}{\langle E \rangle^2} + \left(\frac{\sigma(p)}{p} \right)^2}. \quad (42)$$

Here c refers to the sampling fluctuations, b considers the noise, and $\sigma(p)/p$ denotes the momentum resolution of the beam. In the Monte Carlo the momentum resolution was simulated explicitly. The electronic noise was taken into account by adding random trigger events to the simulated cell energies. The constant c , which is approximately 11% for all modules, was used to simulate the sampling fluctuations.

The simulations were carried out with the H1 detector simulation program H1FAST [20, 21]. The algorithms described so far are part of this program, which is used for the mass production of Monte Carlo events in the H1 detector at the HERA collider at DESY. To keep the required high precision of the parameterization also in complicated detector regions (cracks for example), the following has to be considered. If a shower develops partly inside cracks between adjacent modules, which in general cannot be approximated by a single effective medium, parameterizations will in general fail to reproduce measured signals. In H1FAST⁶ we therefore do not parameterize showers, if they cross such boundaries. Only electromagnetic showers and sub-showers from hadronic interactions are parameterized which fit into one single stack.

During analysis, a 3σ noise cut was applied to both the experimental data and H1FAST data at the cell level, and energy clusters were built from cells containing energies above threshold. Energy distributions of the clusters with maximum channel numbers are compared in Fig.19 for all three modules considered. In addition, the energy in all other cells, not belonging to the selected clusters, are also shown.

⁶A stand alone version (called GFLASH 1.4) running with GEANT and covering the same functionality is available for distribution. Please contact one of the authors.

Longitudinal profiles are shown in Fig.20 for various energies in the IFE calorimeter. The mean profiles as well as the fluctuations are nearly indistinguishable between data and H1FAST. Energy distributions in individual longitudinal layers of CB3 are compared in Fig.21 for 30 GeV incident electron energy, showing that not only the means and fluctuations but also the shape of the distributions are predicted correctly by the parameterized simulations.

Fig.22 compares lateral profiles in different shower depths in the IFE calorimeter at one energy, and in Fig.23 lateral profiles in the FB1 calorimeter, summed over all longitudinal sections, are shown for various energies. There is good agreement in the peak distributions. The tails of the profiles are dominated by electronic noise.

As shown so far, parameterized simulations can predict measured calorimeter signals very precisely, if the shower development is confined within one single calorimeter stack. Using the concept of partial parameterization as described above, the influence of cracks on the measured signal can be reproduced as shown in Fig.24. We have used test beam data scanning the crack between CB2 and CB3, which consist of two electromagnetic (CB2E, CB3E) and two hadronic stacks (CB2H, CB3H). The width of the crack is approximately 1 cm. Shown are the energies in the electromagnetic modules (E_{CB2E} , E_{CB3E}), the sum of both ($E_{CBE} = E_{CB2E} + E_{CB3E}$), and the sum measured in the electromagnetic and hadronic modules ($E_{CB} = E_{CBE} + E_{CBH}$) as a function of the beam impact position. All energies are normalized to $E_{+20} \equiv E_{CB}(x_{calo} = 20cm)$. The energy lost while scanning the crack with a 30 GeV test beam extends to about 40%, if only the electromagnetic sections are considered, and is still around 20% if the hadronic modules are added. The agreement between data and partial parameterization is quite satisfactory.

Of the various comparisons which were made [6], only a limited number is presented here. Other properties, which are relevant for physics analysis with the H1 detector, like e/π separation, were studied [6, 21] and confirm the applicability of the fast simulation.

5 Timing

The CPU time reduction depends on the complexity of the geometry description and the cut off parameters in the detailed simulation as well as on the type of simulated event. Fully parameterized simulations of electromagnetic showers in a simple (box) geometry are about 7000 times faster at 100 GeV (900 at 1 GeV) compared with GEANT simulations of a detailed geometry and with low energy cuts (e -cut= 200 keV, γ -cut= 10 keV).

In the framework of the H1 simulation program, partial parameterization of electromagnetic showers is performed as described above, together with individual tracking of hadrons and termination of low energy particles (see also [20, 21]). The gain factors for 30 GeV showers in the H1 detector (including detailed simulations of tracker volumes) are 200 for electrons and 25 in case of hadronic showers. Medium energy cuts (e -cut= 1 MeV, γ -cut= 200 keV) were used in the corresponding detailed simulations. Complete detector simulations of HERA events (ep scattering at $\sqrt{s} = 314$ GeV) require at least 10 times less CPU time using partial parameterization.

6 Conclusions

We have developed parameterizations of electromagnetic showers for different materials and sampling geometries. Shower to shower fluctuations and correlations are taken into account consistently, as well as correlations between the longitudinal and radial shower development. Comparisons with data have shown that parameterized simulations are able to predict measured calorimeter signals with an acceptable precision. Using the methods described above, the energy resolution is reproduced at the level of $\pm 0.5\%$. The energy deposited in longitudinal and lateral layers is predicted with a precision of typically $\pm 1.5\%$ for both, the means and the fluctuations. Using partial parameterizations, the energy measured in electromagnetic (and hadronic) modules differs by an amount of 1.7% (9%), if the beam enters directly into a crack. The parameterizations presented here provide a fast and precise algorithms for large scale Monte Carlo production of events for physics analysis.

A Summary of formulae

A.1 Homogeneous Media

A.1.1 Average longitudinal profiles

$$\begin{aligned} T_{hom} &= \ln y - 0.858 \\ \alpha_{hom} &= 0.21 + (0.492 + 2.38/Z) \ln y \end{aligned}$$

A.1.2 Fluctuated longitudinal profiles

$$\begin{aligned} \langle \ln T_{hom} \rangle &= \ln(\ln y - 0.812) \\ \sigma(\ln T_{hom}) &= (-1.4 + 1.26 \ln y)^{-1} \\ \langle \ln \alpha_{hom} \rangle &= \ln(0.81 + (0.458 + 2.26/Z) \ln y) \\ \sigma(\ln \alpha_{hom}) &= (-0.58 + 0.86 \ln y)^{-1} \\ \rho(\ln T_{hom}, \ln \alpha_{hom}) &= 0.705 - 0.023 \ln y \end{aligned}$$

A.1.3 Average radial profiles

$$\begin{aligned} R_{C,hom}(\tau) &= z_1 + z_2 \tau \\ R_{T,hom}(\tau) &= k_1 \{ \exp(k_3(\tau - k_2)) + \exp(k_4(\tau - k_2)) \} \\ p_{hom}(\tau) &= p_1 \exp \left\{ \frac{p_2 - \tau}{p_3} - \exp \left(\frac{p_2 - \tau}{p_3} \right) \right\} \end{aligned}$$

with

$$\begin{aligned}
z_1 &= 0.0251 + 0.00319 \ln E \\
z_2 &= 0.1162 + -0.000381 Z \\
k_1 &= 0.659 + -0.00309 Z \\
k_2 &= 0.645 \\
k_3 &= -2.59 \\
k_4 &= 0.3585 + 0.0421 \ln E \\
p_1 &= 2.632 + -0.00094 Z \\
p_2 &= 0.401 + 0.00187 Z \\
p_3 &= 1.313 + -0.0686 \ln E
\end{aligned}$$

A.1.4 Fluctuated radial profiles

$$\begin{aligned}
\tau_i &= \frac{t}{\langle t \rangle_i} \frac{\exp(\langle \ln \alpha \rangle)}{\exp(\langle \ln \alpha \rangle) - 1} \\
N_{Spot} &= 93 \ln(Z) E^{0.876} \\
T_{Spot} &= T_{hom}(0.698 + 0.00212 Z) \\
\alpha_{Spot} &= \alpha_{hom}(0.639 + 0.00334 Z)
\end{aligned}$$

A.2 Sampling Calorimeters

A.2.1 Material and geometry parameters

$$\begin{aligned}
w_i &= \frac{\rho_i d_i}{\sum_j \rho_j d_j} \quad (\rho = \text{density}) \\
Z_{eff} &= \sum_i w_i Z_i \\
A_{eff} &= \sum_i w_i A_i \\
\frac{1}{X_{0,eff}} &= \sum_i \frac{w_i}{X_{0,i}} \\
\frac{1}{R_{M,eff}} &= \frac{1}{E_s} \sum_i \frac{w_i E_{c,i}}{X_{0,i}} \quad (E_s = 21.2 \text{ MeV}) \\
E_{c,eff} &= X_{0,eff} \sum_i \frac{w_i E_{c,i}}{X_{0,i}} \\
F_S &= \frac{X_{0,eff}}{d_a + d_p} \\
\hat{e} &= \frac{1}{1 + 0.007(Z_p - Z_a)}
\end{aligned}$$

A.2.2 Average longitudinal profiles

$$\begin{aligned} T_{sam} &= T_{hom} - 0.59F_S^{-1} - 0.53(1 - \hat{e}) \\ \alpha_{sam} &= \alpha_{hom} - 0.444F_S^{-1} \end{aligned}$$

A.2.3 Fluctuated longitudinal profiles

$$\begin{aligned} \langle \ln T_{sam} \rangle &= \ln \left(\exp(\langle \ln T_{hom} \rangle) - 0.55F_S^{-1} - 0.69(1 - \hat{e}) \right) \\ \sigma(\ln T_{sam}) &= (-2.5 + 1.25 \ln y)^{-1} \\ \langle \ln \alpha_{sam} \rangle &= \ln \left(\exp(\langle \ln \alpha_{hom} \rangle) - 0.476F_S^{-1} \right) \\ \sigma(\ln \alpha_{sam}) &= (-0.82 + 0.79 \ln y)^{-1} \\ \rho(\ln T_{sam}, \ln \alpha_{sam}) &= 0.784 - 0.023 \ln y \end{aligned}$$

A.2.4 Average radial profiles

$$\begin{aligned} R_{C,sam} &= R_{C,hom} - 0.0203(1 - \hat{e}) + 0.0397F_S^{-1} \exp(-\tau) \\ R_{T,sam} &= R_{T,hom} - 0.14(1 - \hat{e}) - 0.495F_S^{-1} \exp(-\tau) \\ p_{sam} &= p_{hom} + (1 - \hat{e})(0.348 - 0.642F_S^{-1} \exp(-(\tau - 1)^2)) \end{aligned}$$

A.2.5 Fluctuated radial profiles

$$\begin{aligned} \tau_i &= \frac{t}{\langle t \rangle_i} \frac{\exp(\langle \ln \alpha \rangle)}{\exp(\langle \ln \alpha \rangle) - 1} \\ N_{Spot} &= \frac{10.3}{c} E^{0.959} \quad \left(\frac{\sigma}{E} = \frac{c}{\sqrt{E}} \right) \\ T_{Spot} &= T_{hom}(0.813 + 0.0019Z) \\ \alpha_{Spot} &= \alpha_{hom}(0.844 + 0.0026Z) \end{aligned}$$

References

- [1] E. Longo and I. Sestili, Nucl. Instrum. Meth. 128, 283, (1975).
- [2] R. K. Bock et al., Nucl. Instrum. Meth. 186, 533, (1981);
M. della Negra, Scripta Phys. 23, 469, (1981).
- [3] Y. Hayashide et al., CDF Note 287, Batavia, IL (1985).
- [4] J. Badier and M. Bardadin-Otwinowska, ALEPH 87–9, EMCAL 87–1, Geneva (1987).
- [5] G. Grindhammer, M. Rudowicz, and S. Peters, Nucl. Instrum. Meth. A290, 469, (1990).
- [6] S. Peters, PhD thesis, University of Hamburg; MPI–PhE/92–13 (1992).
- [7] R. Brun et al., GEANT3 User’s Guide. CERN–DD/EE 84–1, Geneva (1986).
- [8] W. Flauger, Nucl. Instrum. Meth. A241, 72, (1985).
- [9] R. Wigmans, Nucl. Instrum. Meth. A259, 389, (1987).
- [10] B. Rossi, Prentice Hall, New York, (1952).
- [11] O. I. Dovzhenkko and A. A. Pommanskii, Sov. Phys. JETP Vol. 18, Numb. 1, (1964).
- [12] J. del Peso and E. Ros, Nucl. Instrum. Meth. A295, 330, (1990).
- [13] H1 Collab., Technical Proposal for the H1 Detector, DESY, (1986);
H1 Collab., I. Abt et al., Nucl. Instrum. Meth. A386, 310 and A386, 348, (1997).
- [14] G. A. Akopdjanov et al., Nucl. Instrum. Meth. 140, 441, (1977).
- [15] G. Abshire et al., Nucl. Instrum. Meth. 164, 67, (1979).
- [16] G. Ferri et al., Nucl. Instrum. Meth. A273, 123, (1988).
- [17] J. del Peso and E. Ros, Nucl. Instrum. Meth. A276, 456, (1989).
- [18] SICAPO Collab., E. Borchini et al., Nucl. Phys. Proc. Suppl. 23A, 119, (1991).
- [19] A. de Angelis and P. A. Palazzi, Nucl. Instrum. Meth. A271, 455, (1988).
- [20] M. Kuhlen, in Proceedings of the XXVI International Conference on High Energy Physics, Dallas (1992).
- [21] M. Rudowicz, PhD thesis, University of Hamburg; MPI–PhE/92–14 (1992).

Figure Captions

1	Depths of the shower maxima as a function of y (GEANT).	19
2	Shape parameter α as a function of y (GEANT).	20
3	Parameters of longitudinal profiles in homogeneous media (GEANT)	21
4	Mean longitudinal profiles and their fluctuations in a lead glass calorimeter (GEANT and param. simulation)	22
5	Parameters of individual longitudinal energy profiles in sampling calorimeters (GEANT)	23
6	Mean longitudinal profiles and their fluctuations in the H1 lead liquid argon calorimeter IFE (H1-IFE) (GEANT and param. simulation)	24
7	Energy containment vs. calorimeter depth in H1-IFE (GEANT and param. simulation)	25
8	Energy resolution vs. calorimeter depth in H1-IFE (GEANT and param. simulation)	26
9	Mean radial profiles in uranium at various calorimeter depth (GEANT). The two component Ansatz is indicated for the depth $1 - 2X_0$	27
10	Shower depth and material dependence of radial shower parameters	28
11	Tungsten, 40 GeV. Left figure: Decomposition of the two sources of radial shape fluctuations. Right figure: Comparison of energy and spot density distributions	29
12	Mean radial profiles and their fluctuations in lead (40 GeV) and uranium (100 GeV) (GEANT and param. simulation)	30
13	Top: Mean integrated radial profiles in lead glass. Bottom: Corresponding shape fluctuations: — (···) with (without) long./rad. correlations (GEANT and param. simulation)	31
14	Total number of spots required to reproduce radial shape fluctuations in sampling calorimeters	32
15	Mean radial profiles in H1-IFE (GEANT and param. simulation)	33
16	Radial shape fluctuations in H1-IFE (GEANT and param. simulation)	34
17	Energy containment vs. calorimeter radius in H1-IFE (GEANT and param. simulation)	35
18	Energy resolution vs. calorimeter radius in H1-IFE: — (···) with (without) long./rad. correlations (GEANT and param. simulation)	36
19	Energy distributions of the cluster with the maximum number of channels (E_{max}) and of all other channels (E_{rest}) for 30 GeV showers in three different modules, IFE, CB3, and FB1 of the H1 lead liquid argon calorimeter (data and H1FAST)	37
20	Mean longitudinal profiles and fluctuations in H1-IFE (data and H1FAST)	38
21	Energy distributions in 4 subsequent layers of H1-CB3 for 30 GeV (data and H1FAST)	39

22	Mean lateral profiles and fluctuations at different depths in H1-IFE for 10 GeV (data and H1FAST). The coordinates J correspond to transverse pad numbers	40
23	Mean lateral profiles and fluctuations in H1-FB1 (data and H1FAST). The coordinates I correspond to transverse pad numbers	41
24	Normalized energies as measured across a crack between the modules H1-CB2 and H1-CB3 (data and H1FAST)	42

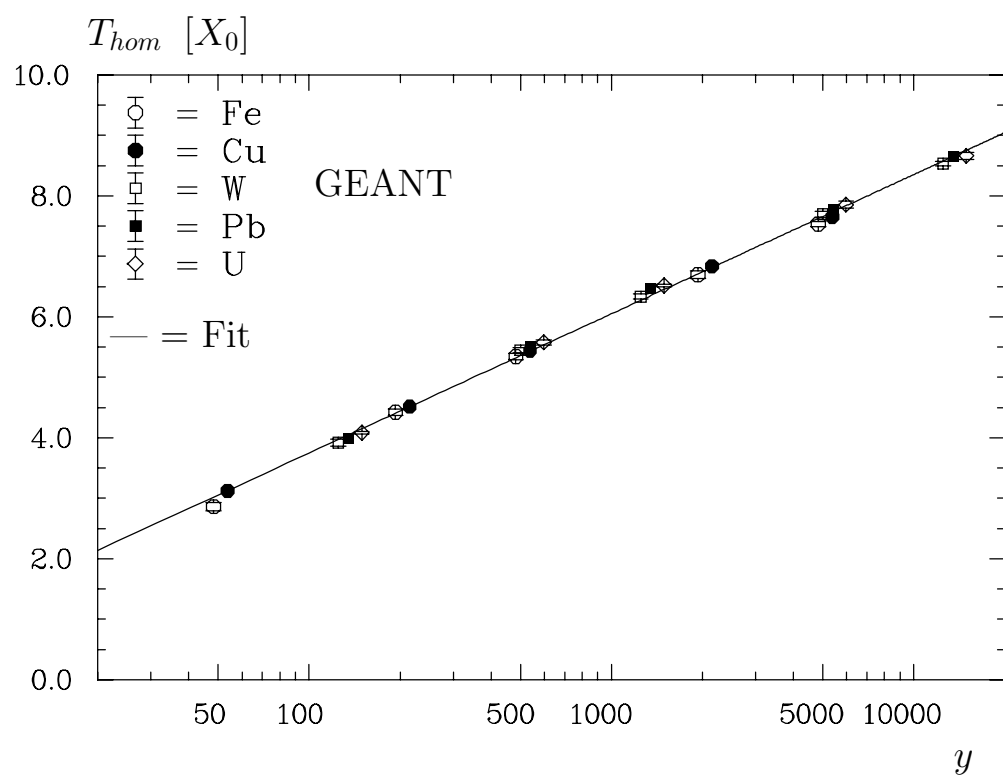


Figure 1:

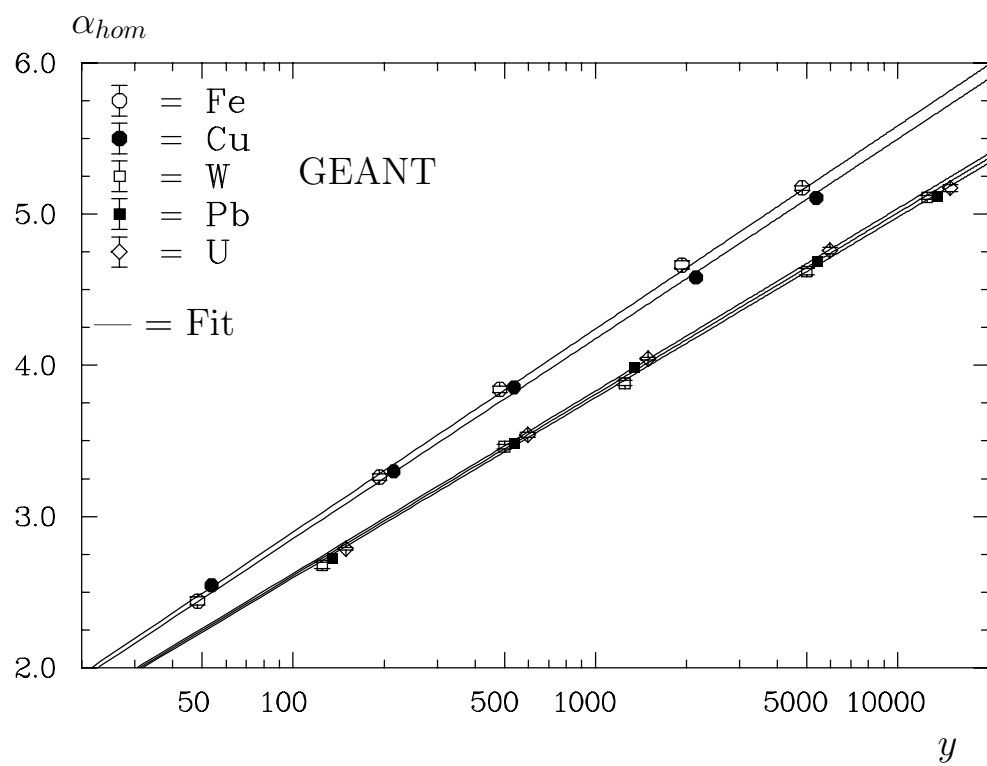


Figure 2:

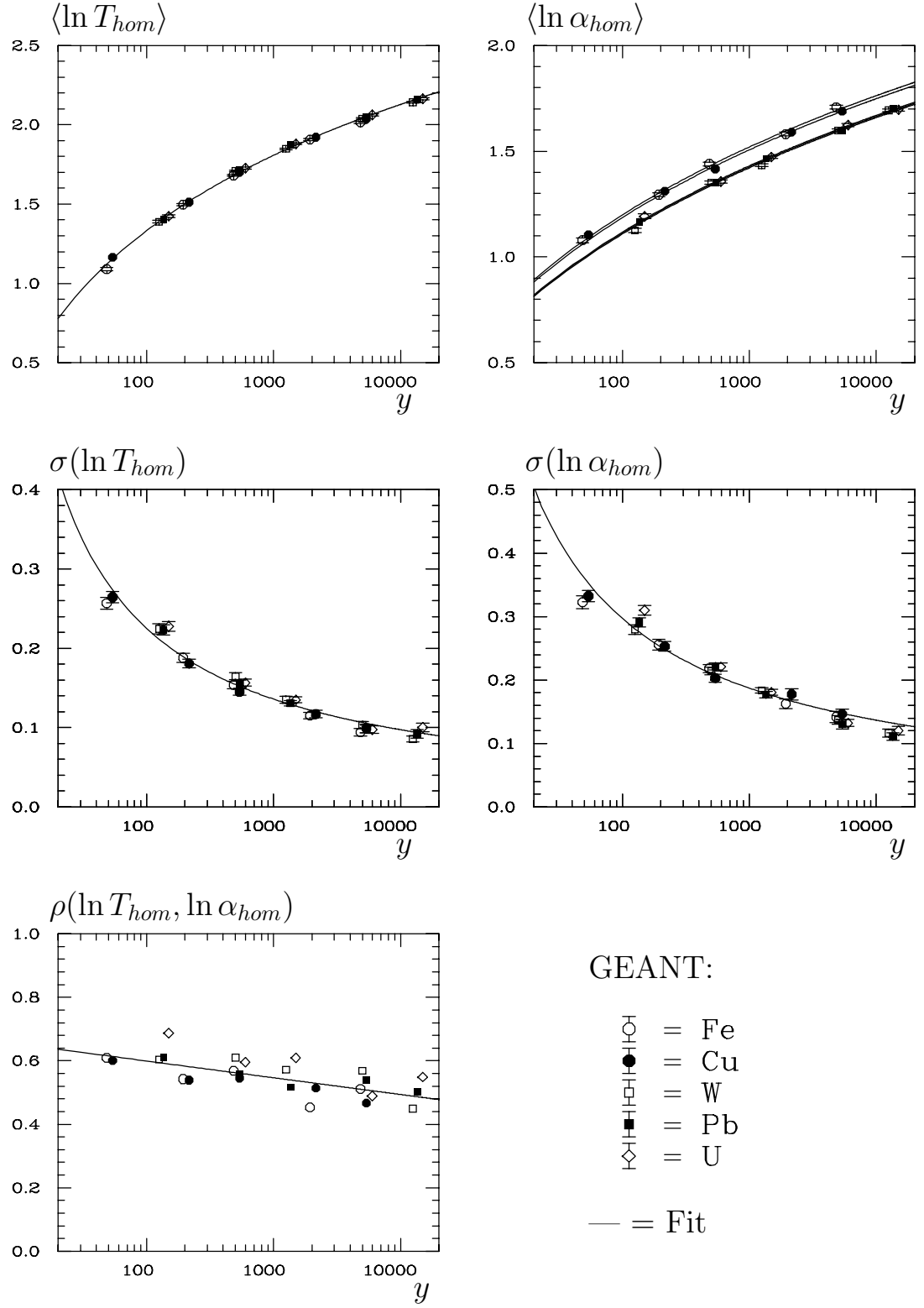


Figure 3:

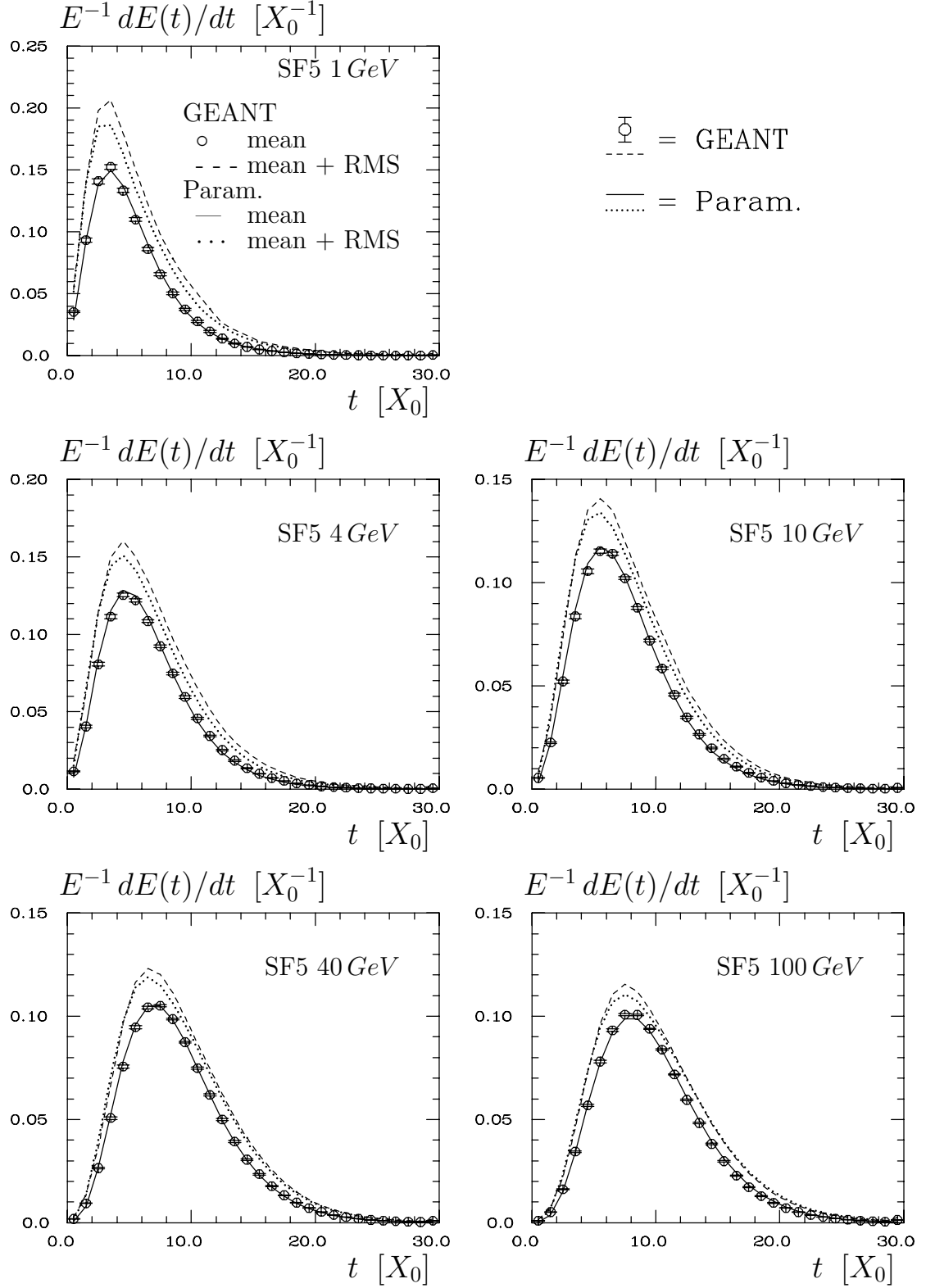


Figure 4:

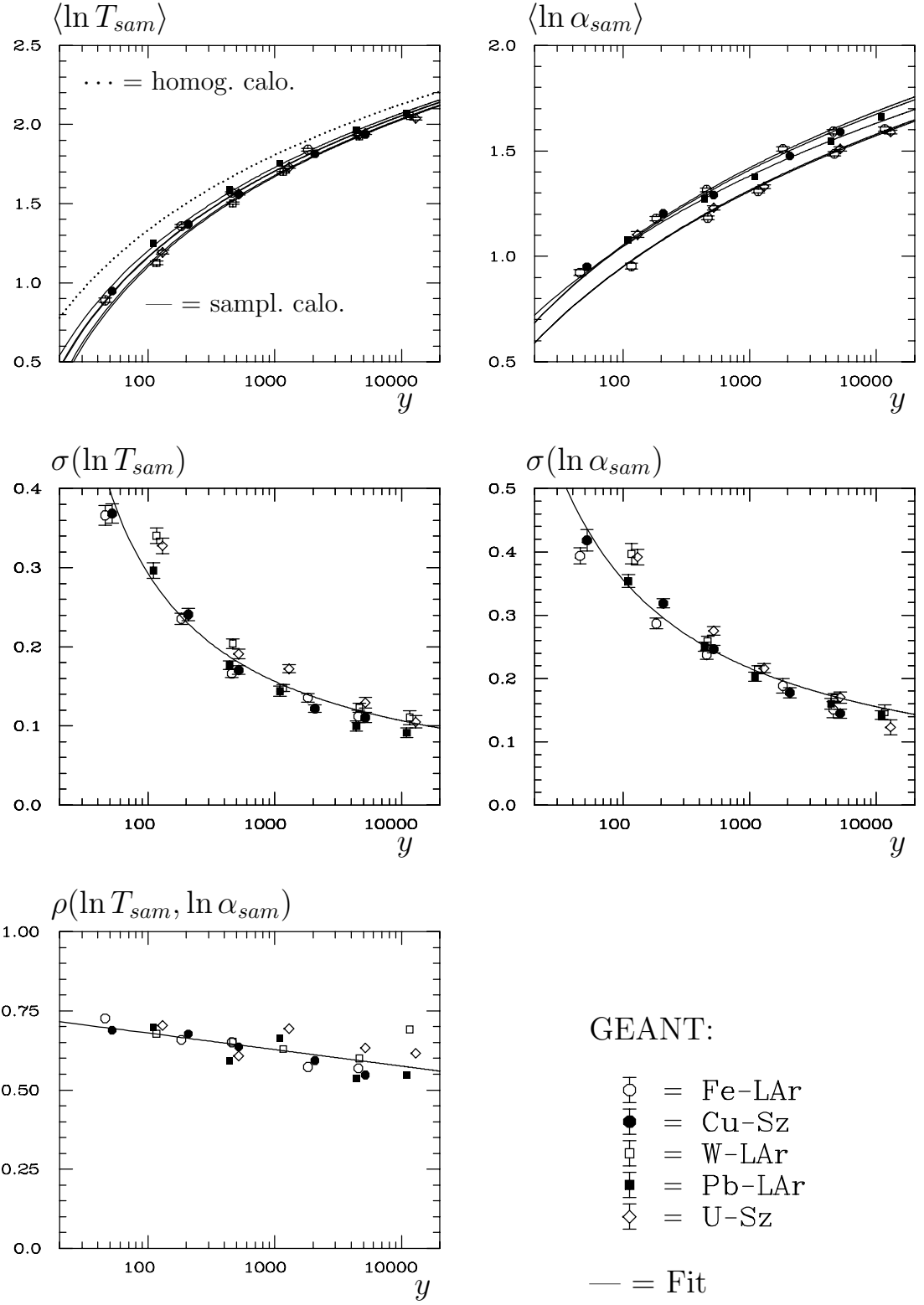


Figure 5:

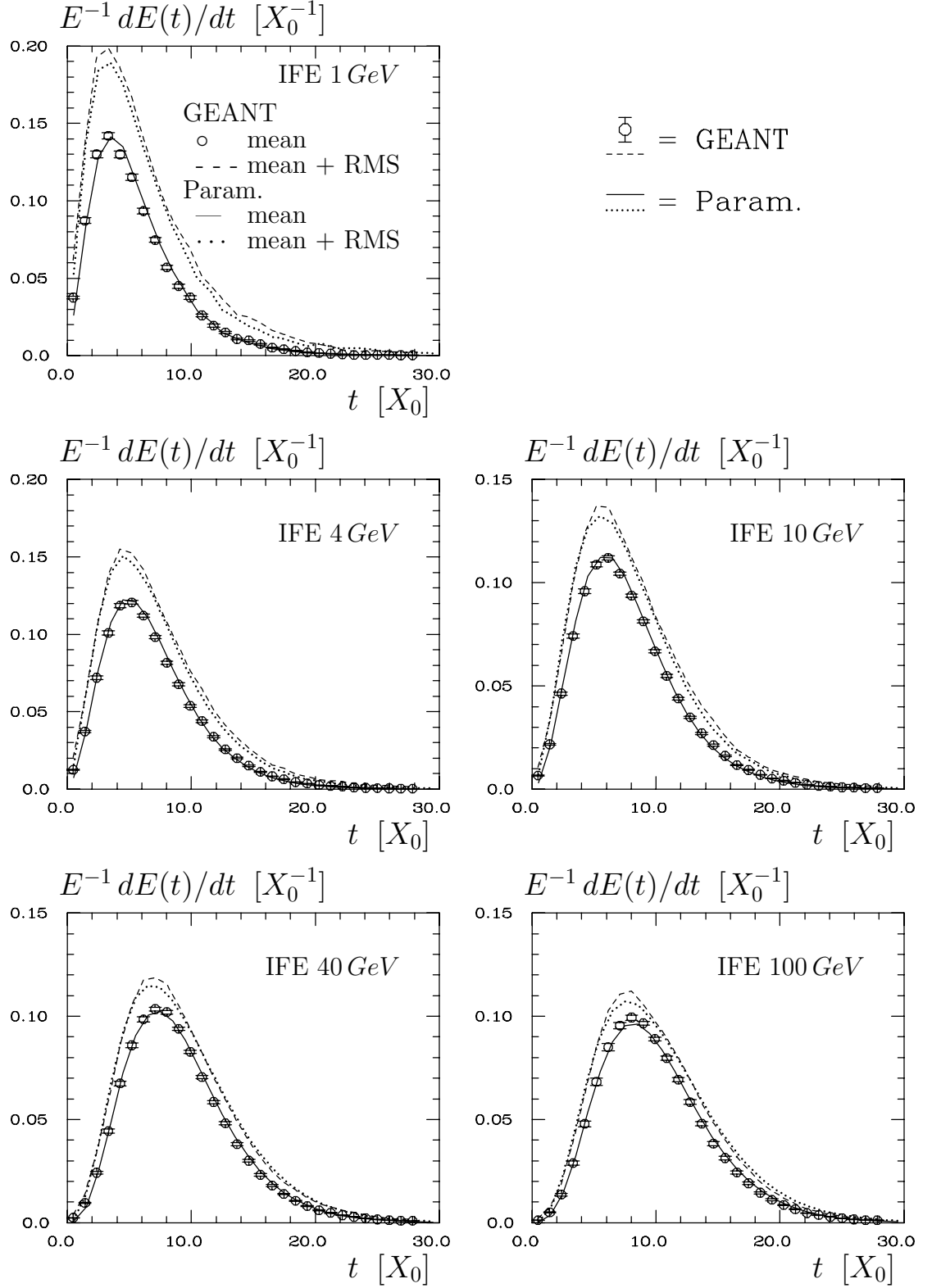


Figure 6:

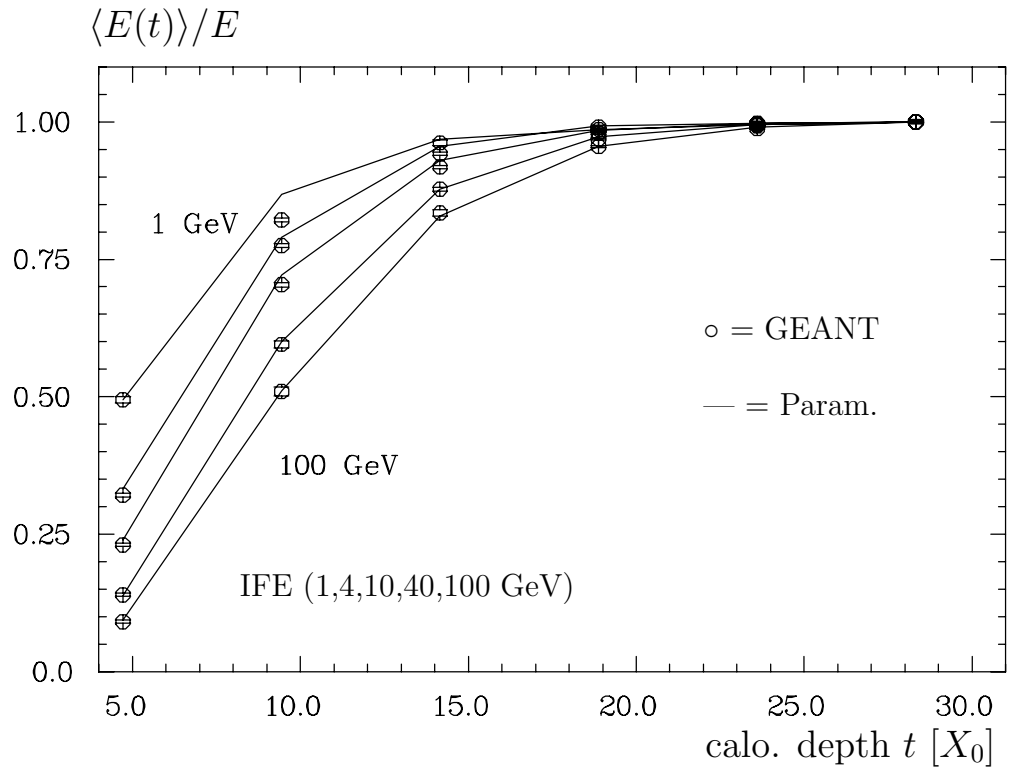


Figure 7:

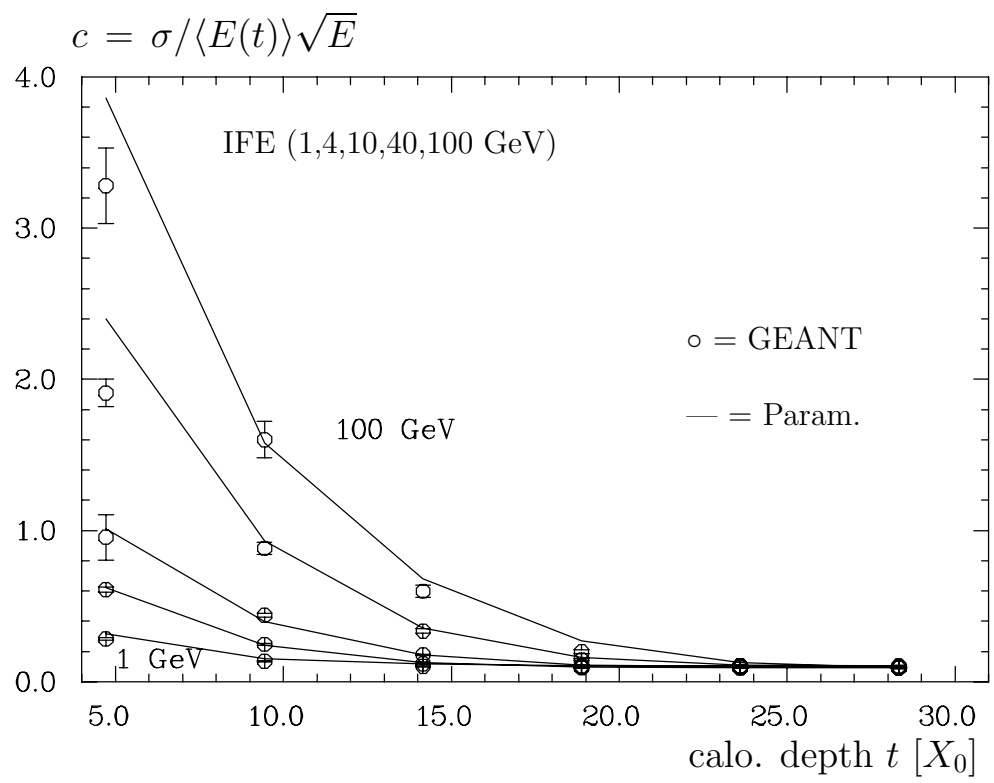


Figure 8:

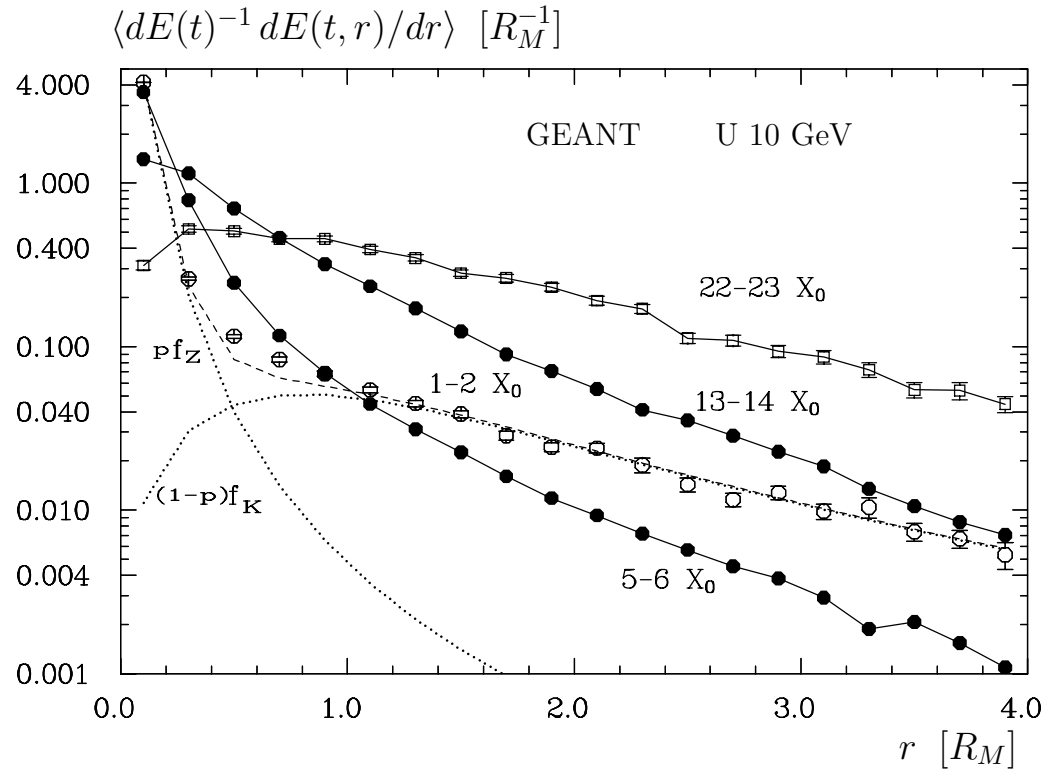


Figure 9:

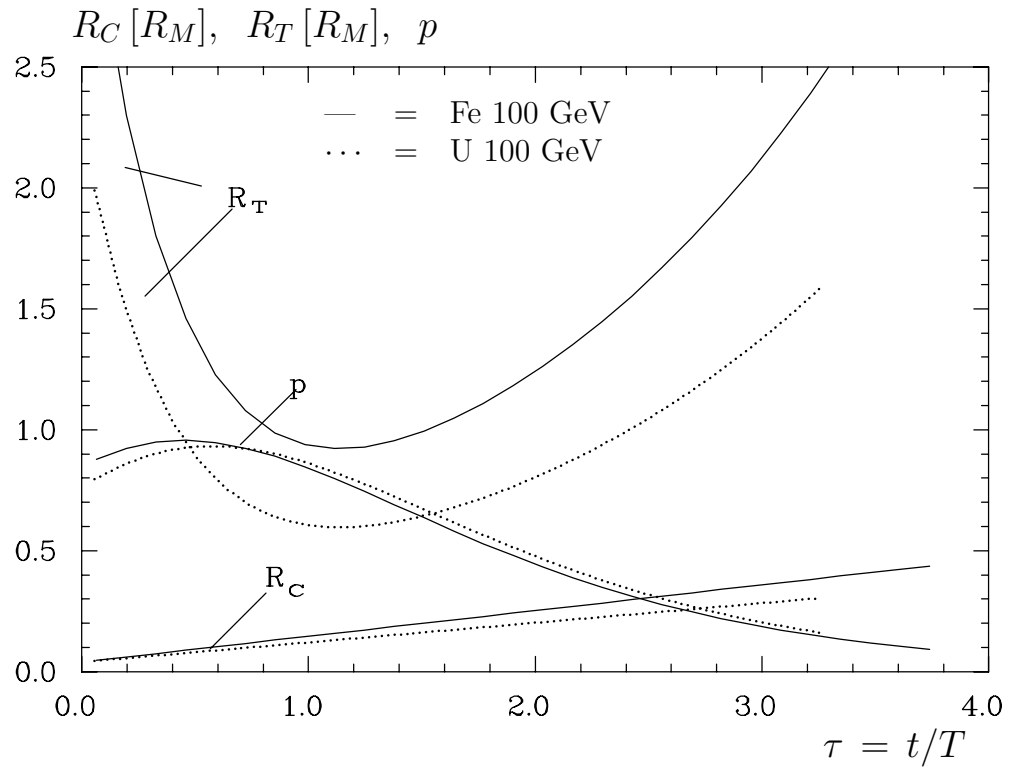


Figure 10:

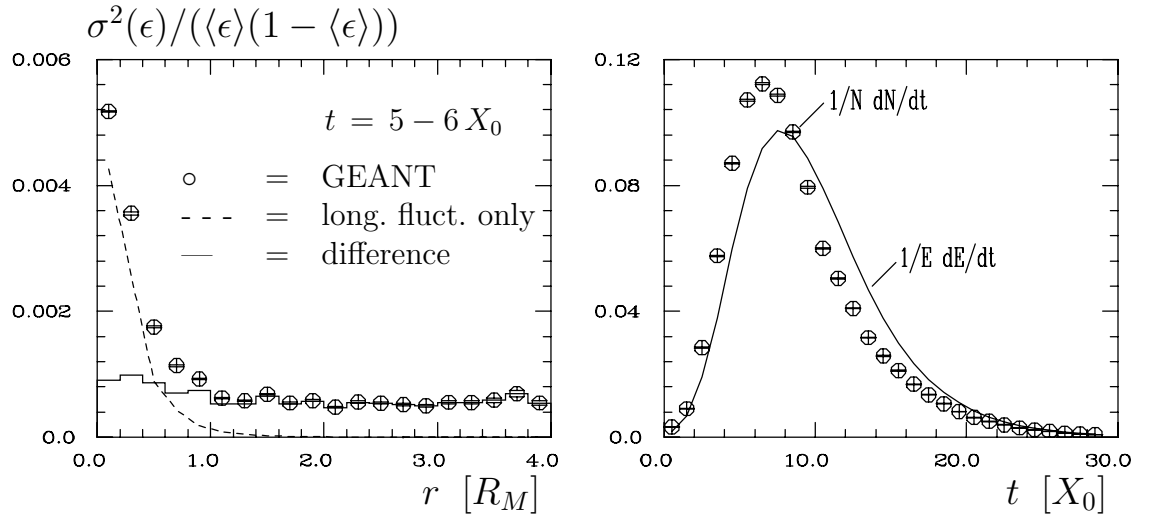


Figure 11:

40 GeV

100 GeV

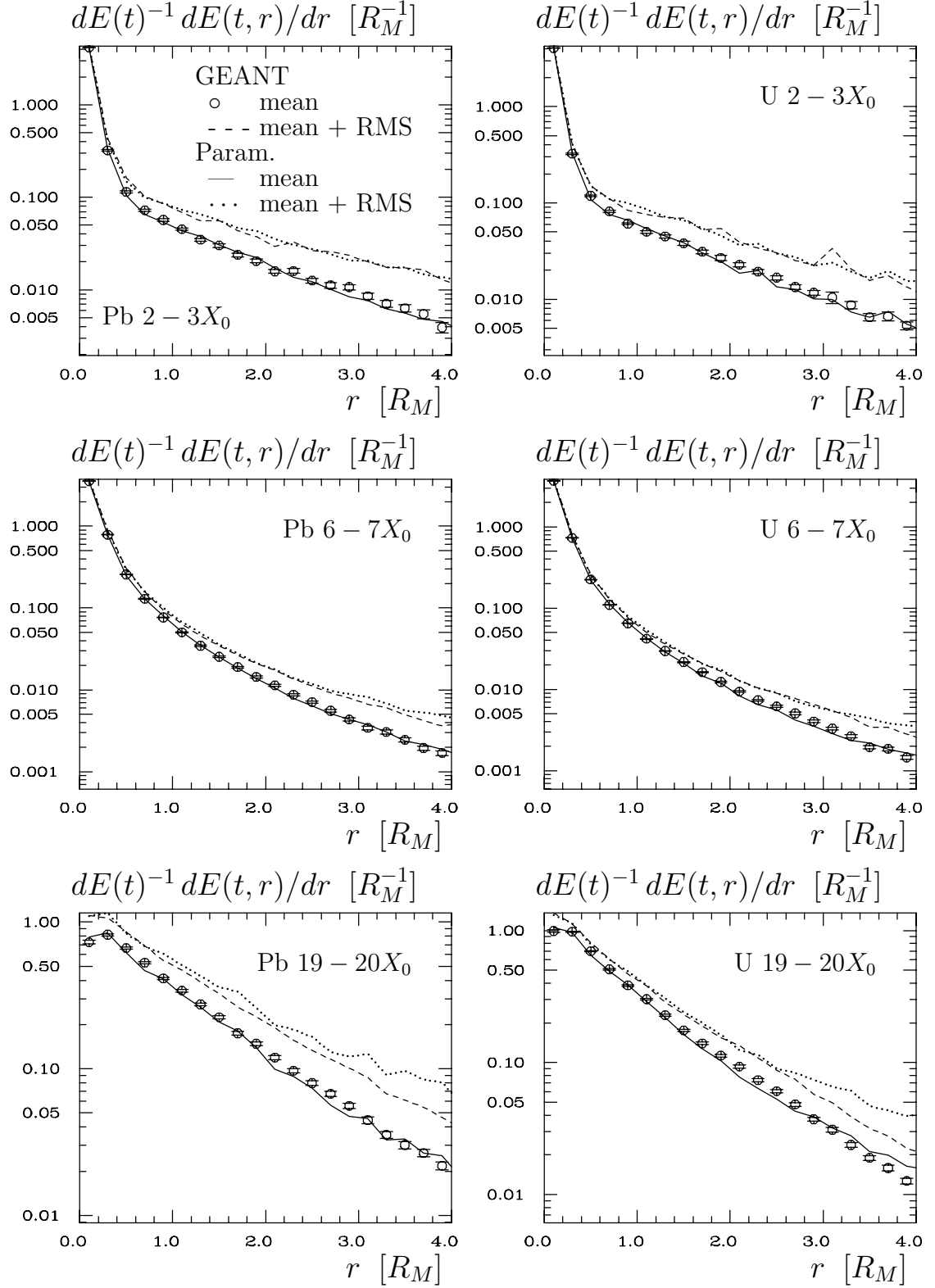


Figure 12:

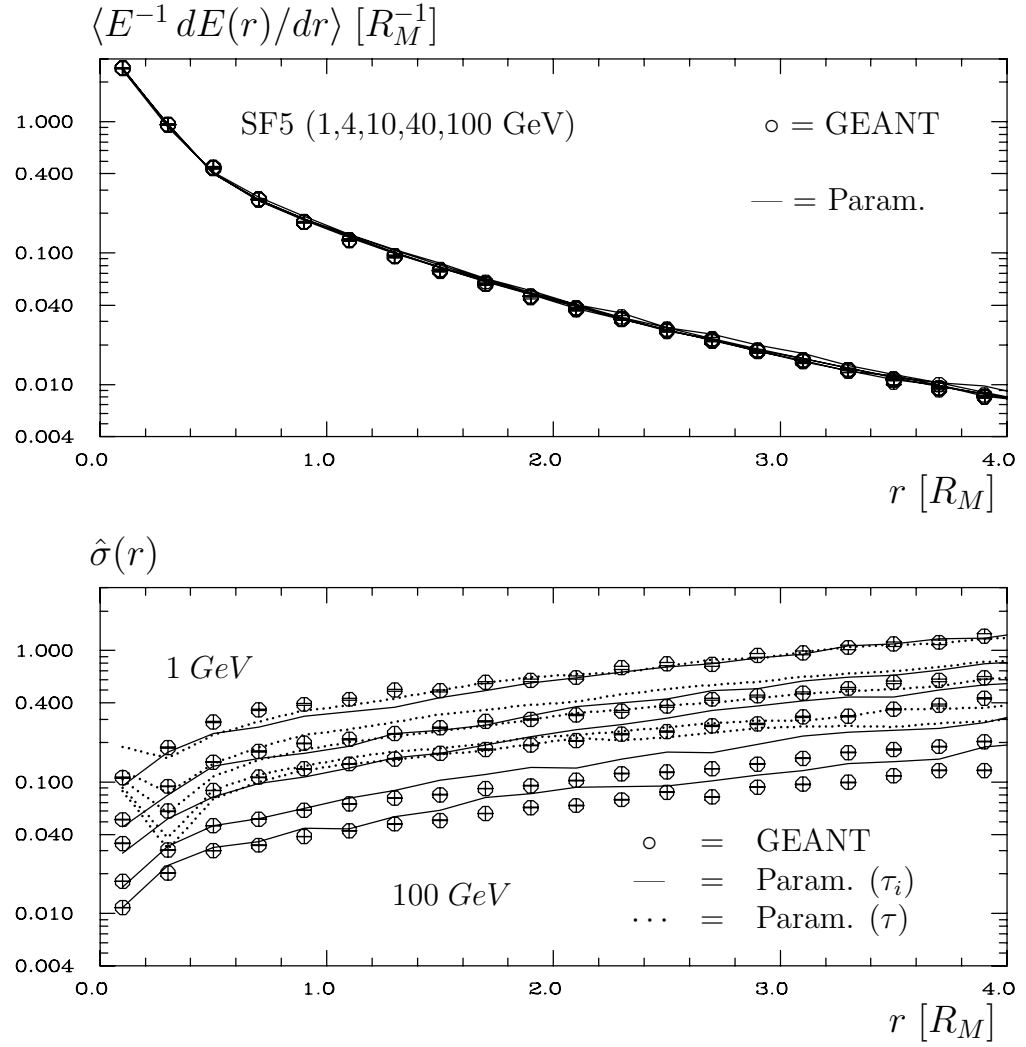


Figure 13:

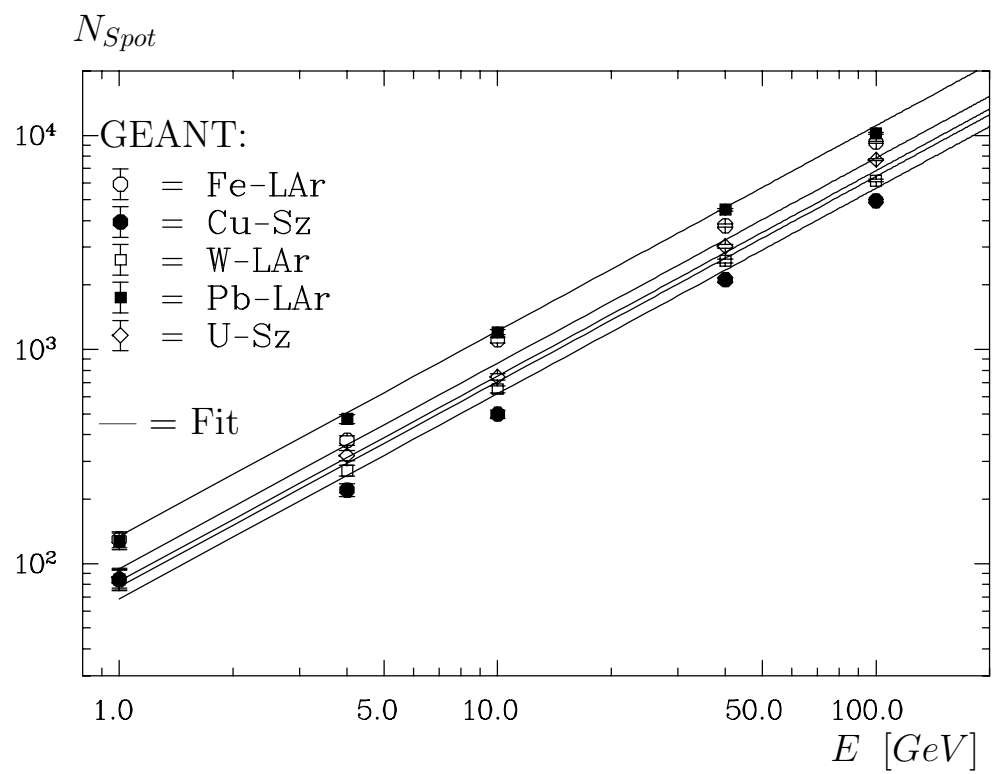
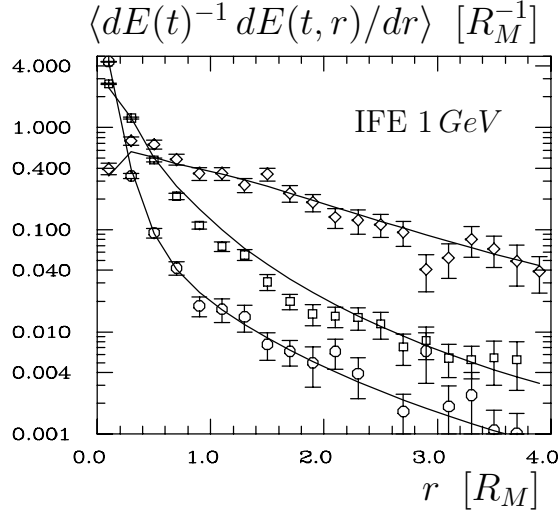


Figure 14:



GEANT:

- \circ = 1-2 X_0 / 2-3 X_0
- \square = 5-6
- \diamond = 14-15 X_0
- \triangle = 24-25 X_0

Param.: —

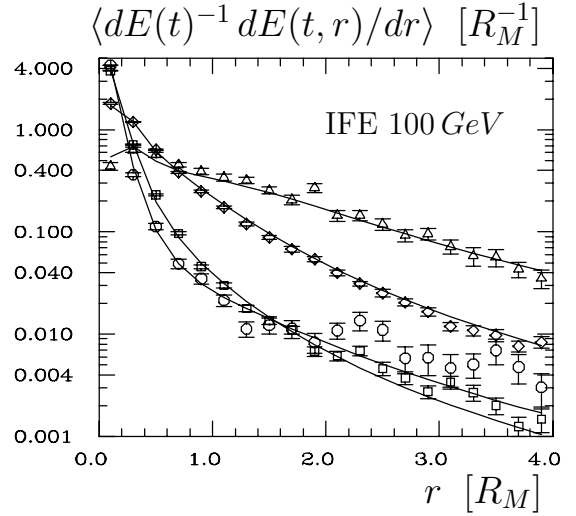
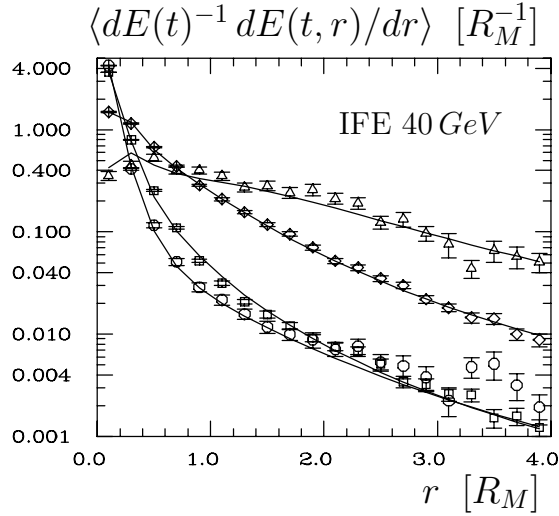
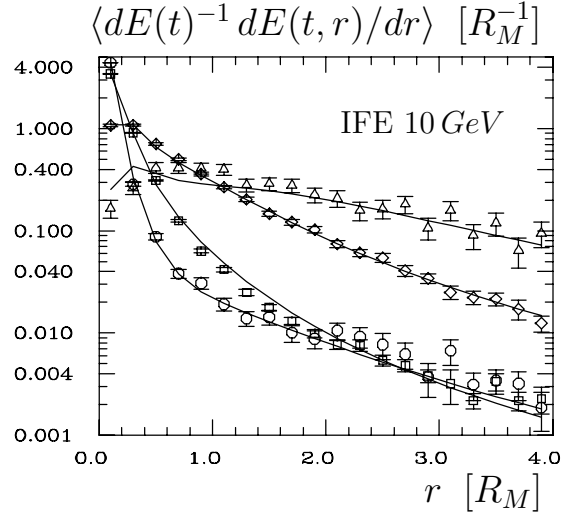
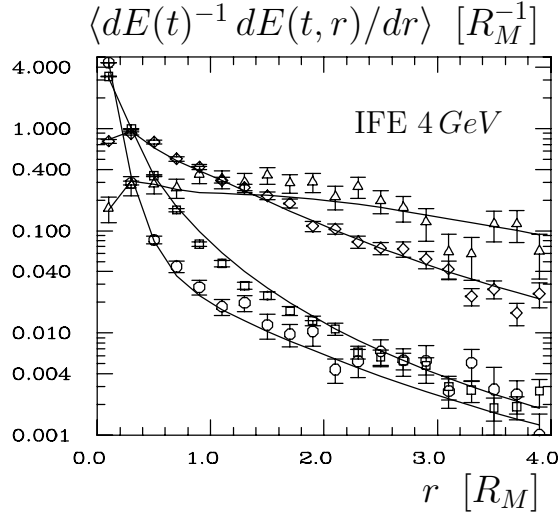
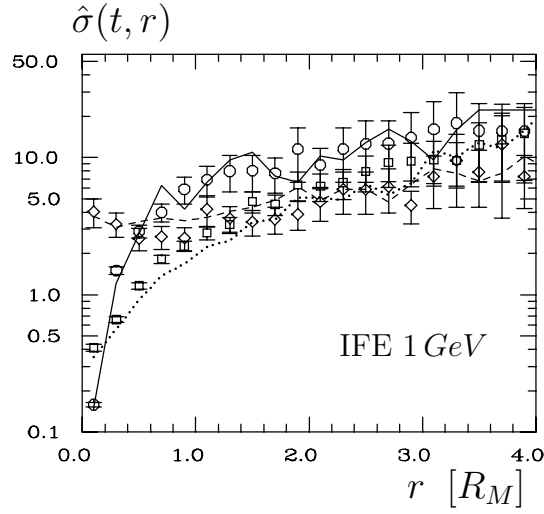


Figure 15:



GEANT:

○ = 1-2 X_0 / 2-3 X_0
 □ = 5-6 X_0
 ◇ = 17-18 X_0

Param.: —, ···, ---

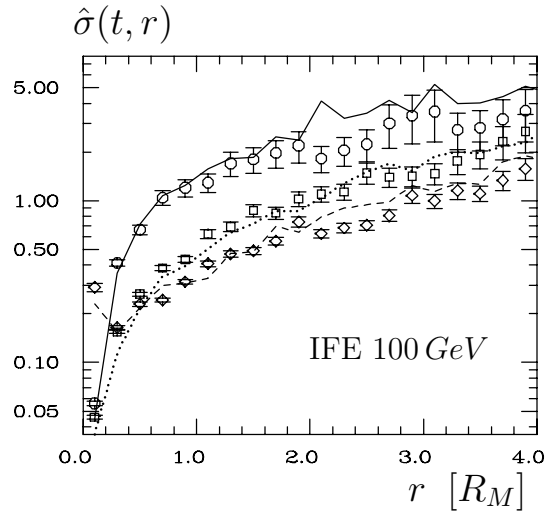
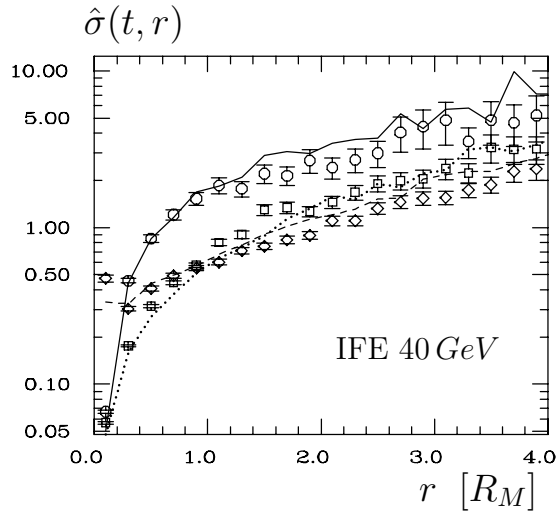
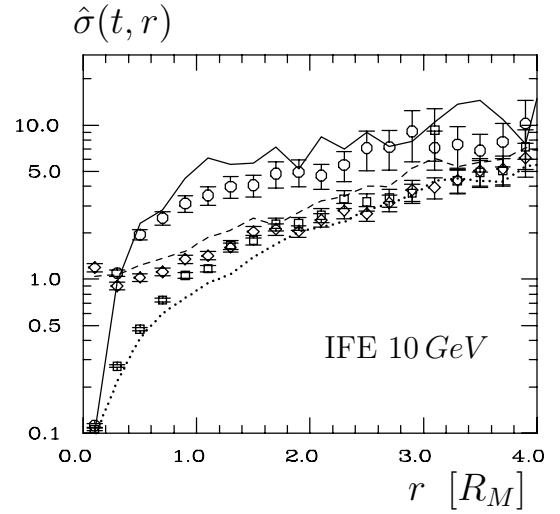
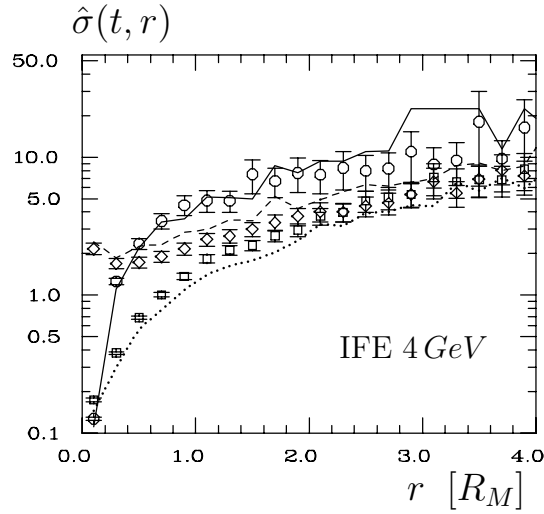


Figure 16:

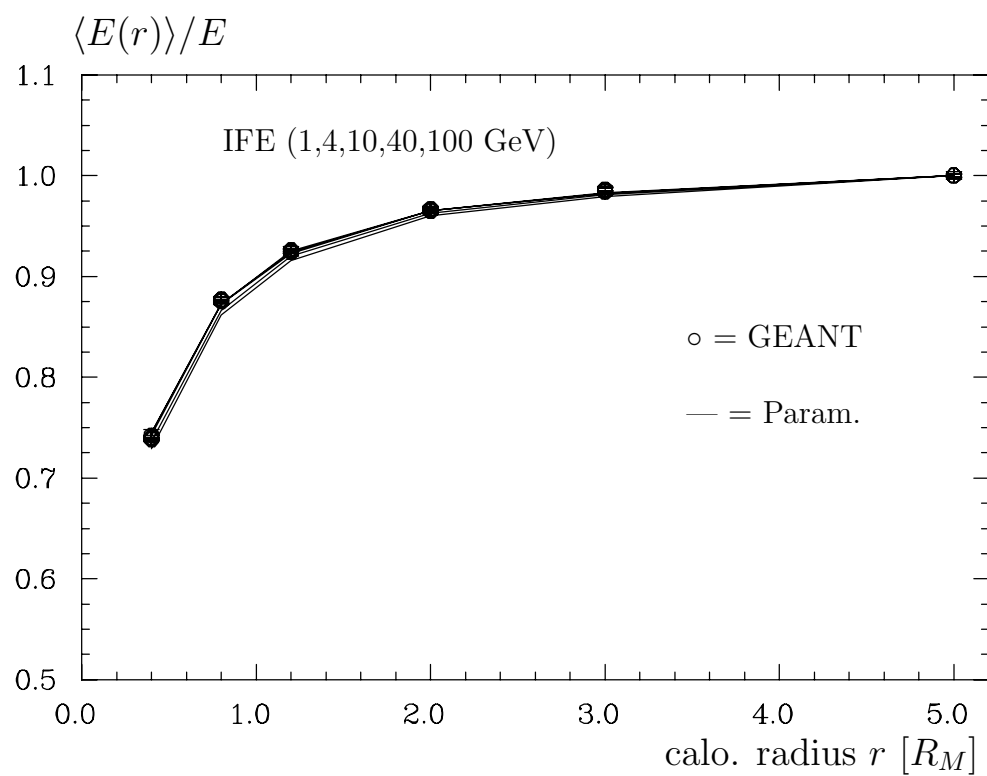


Figure 17:

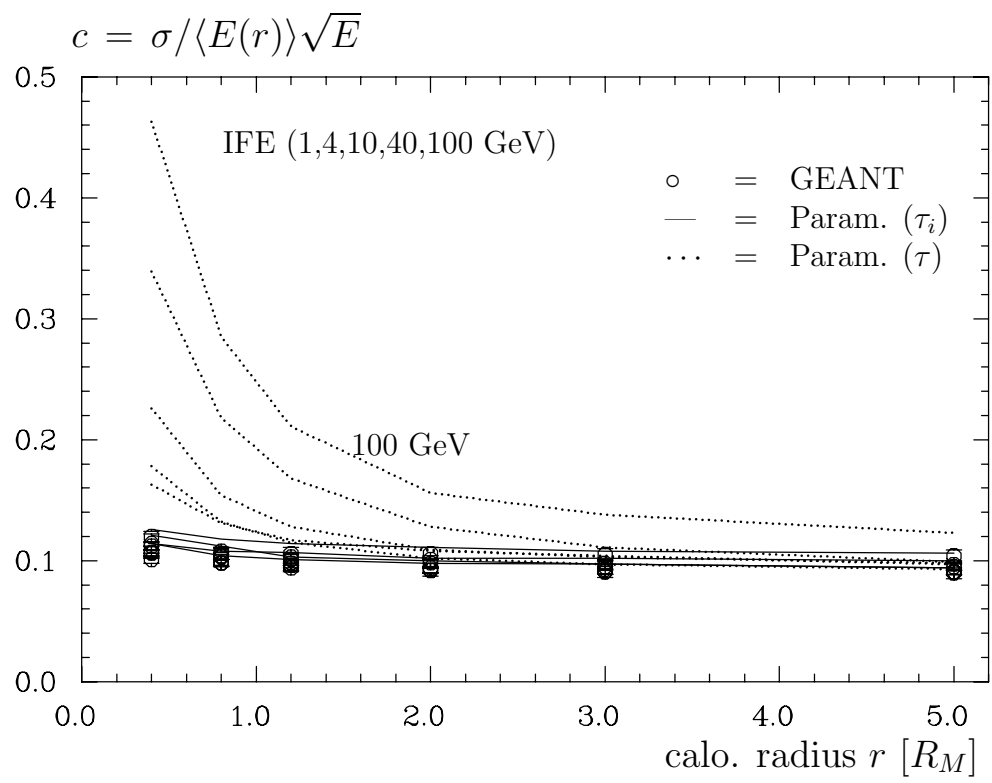


Figure 18:

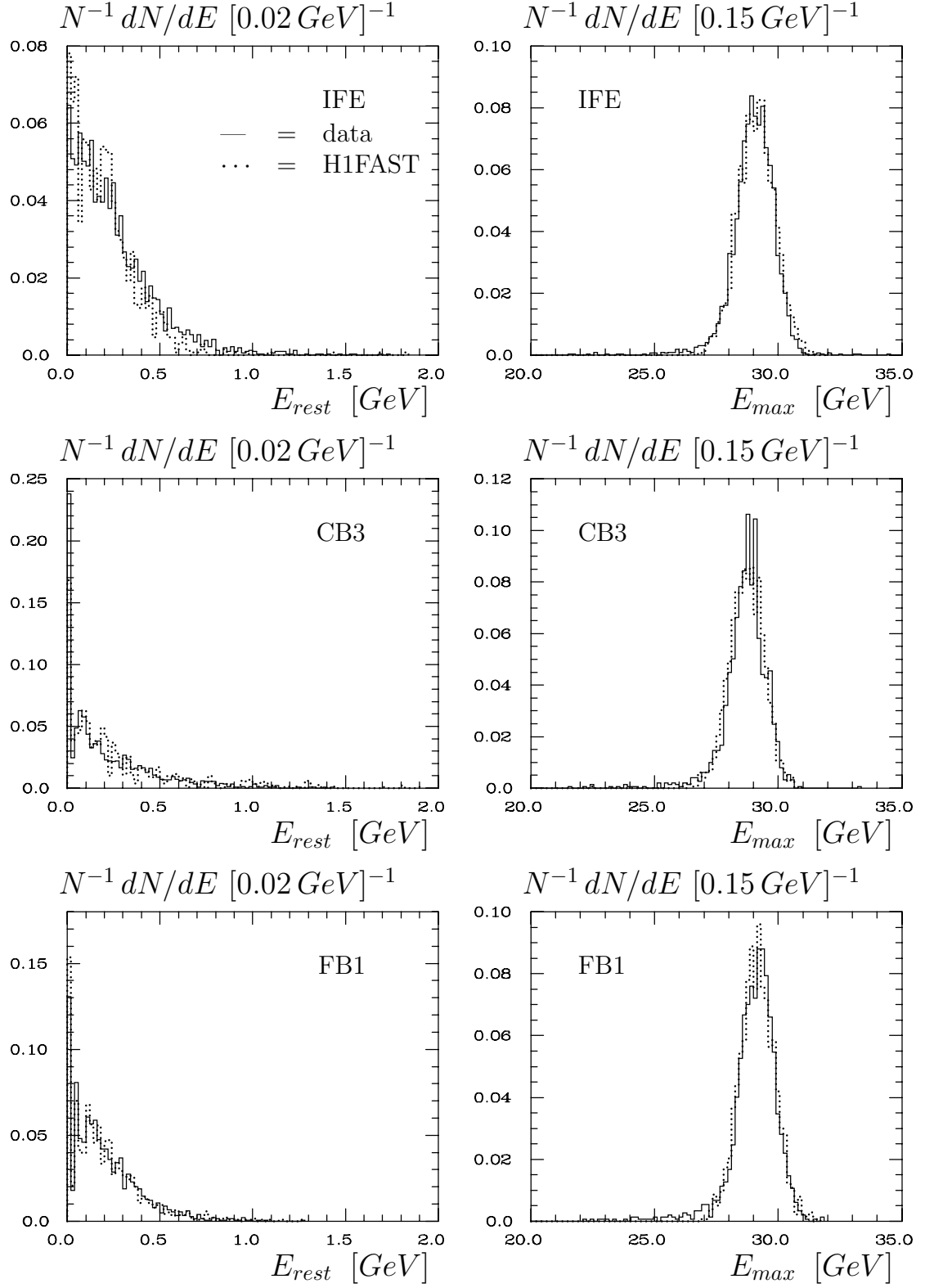


Figure 19:

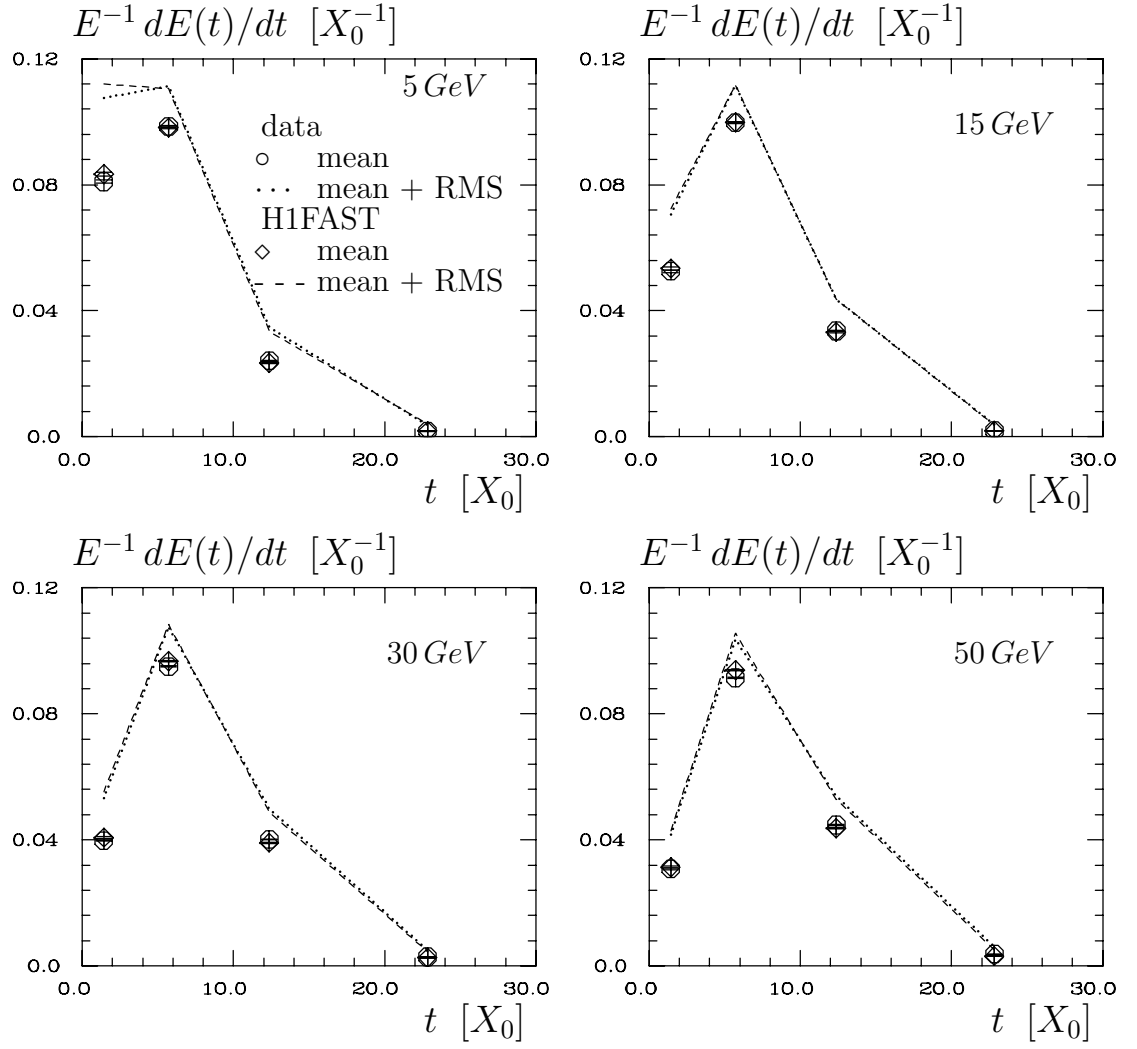


Figure 20:

30 GeV

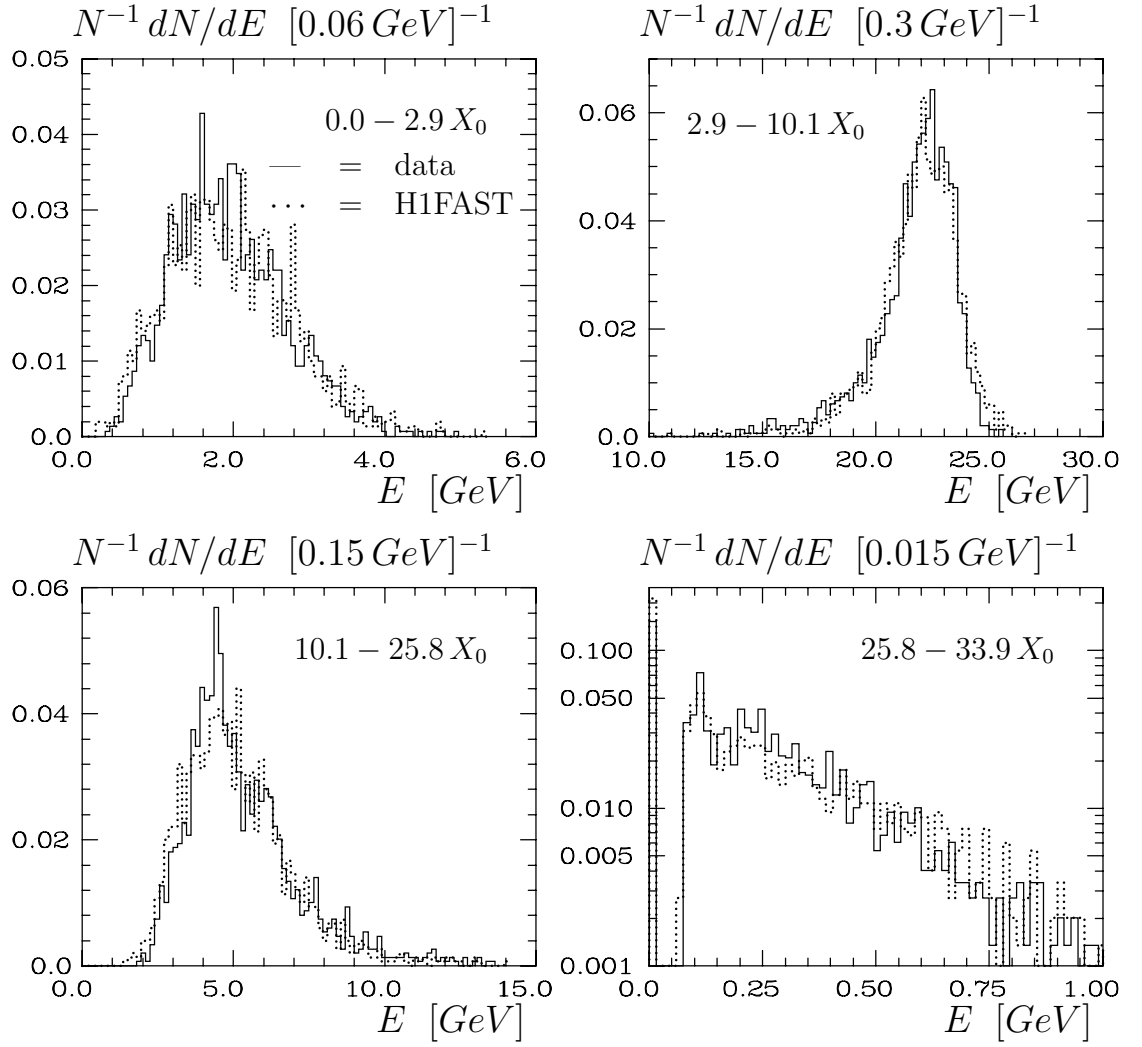


Figure 21:

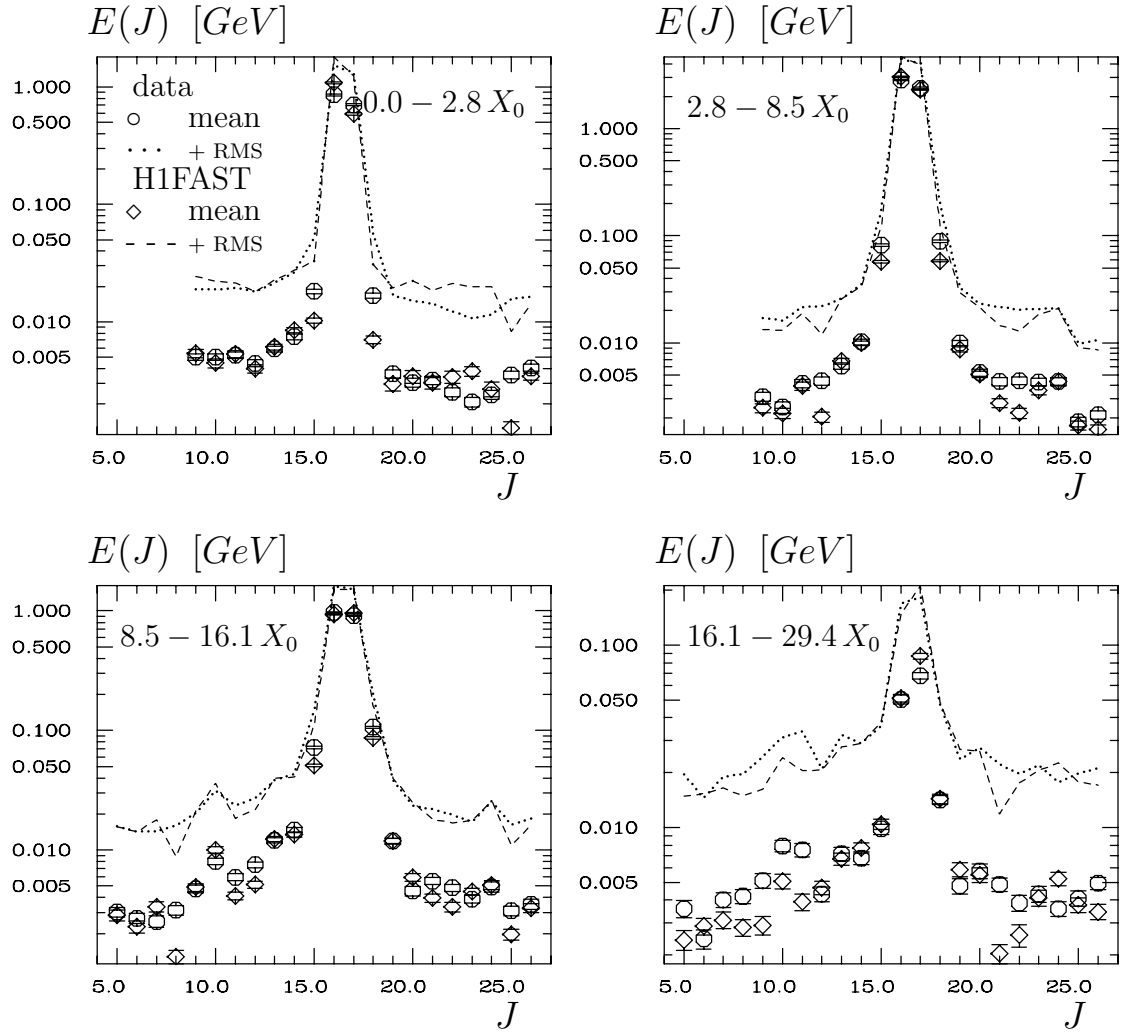


Figure 22:

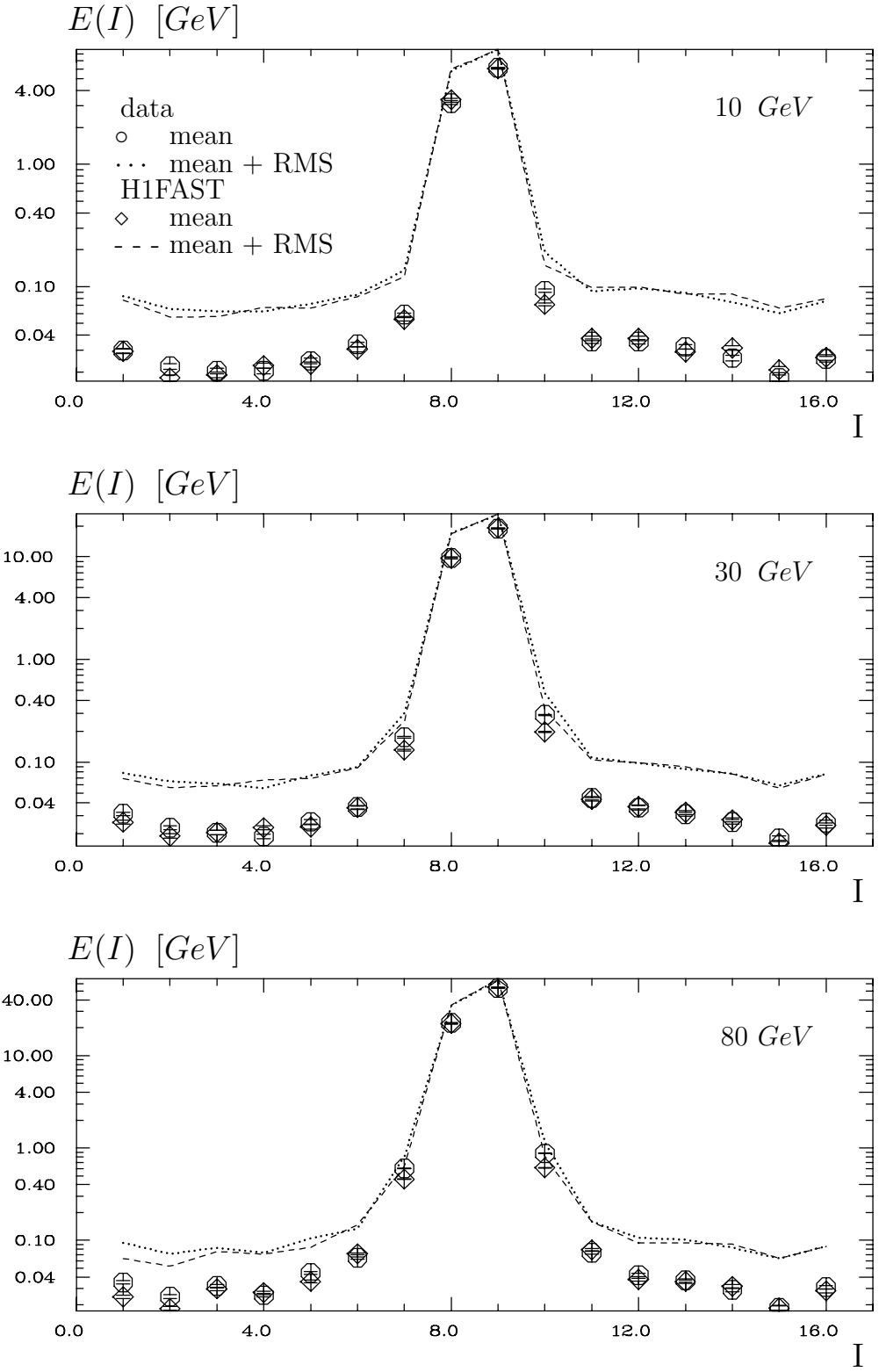


Figure 23:

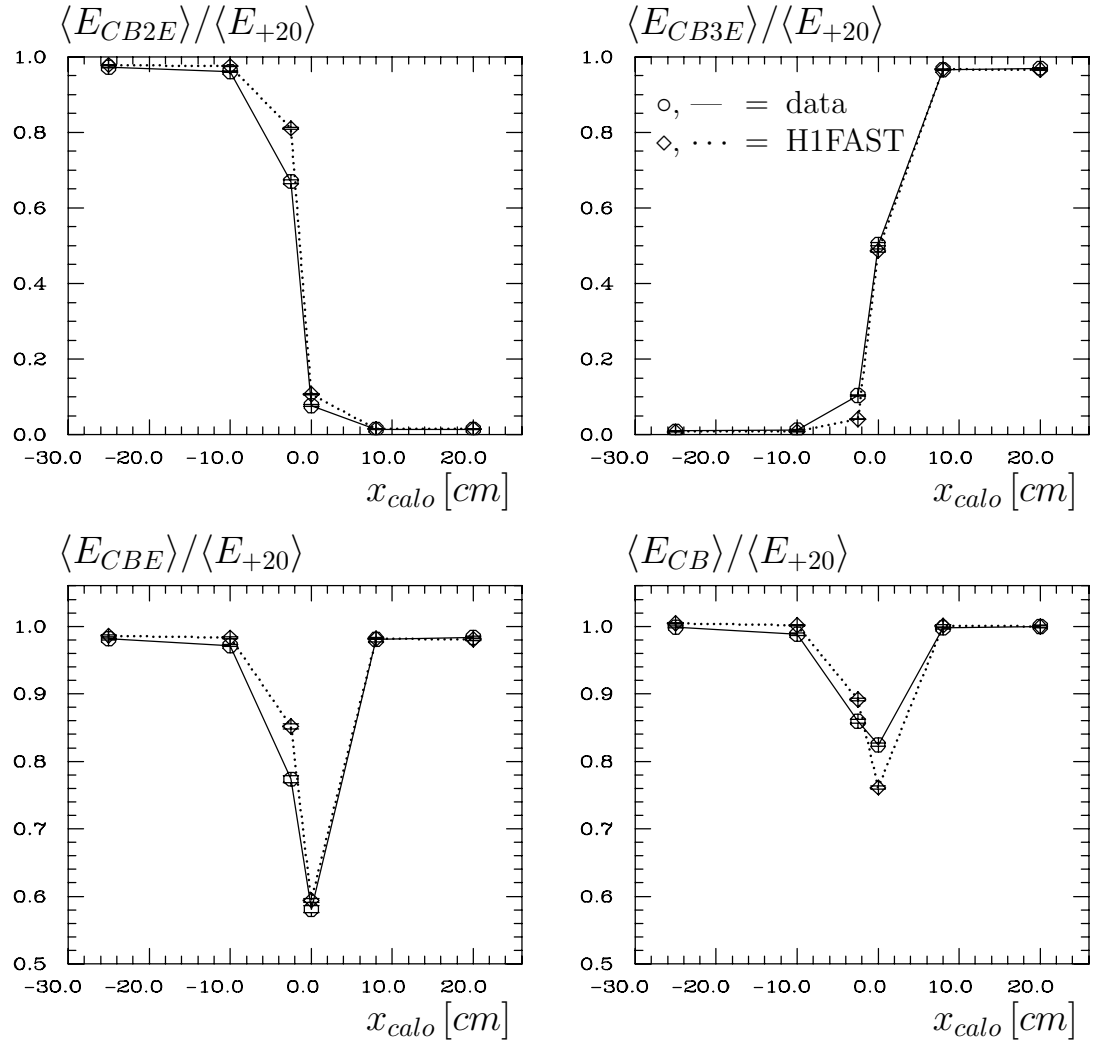


Figure 24: